Wrinkling instabilities of swelling hydrogels

Joseph J. Webber[*,†] and M. Grae Worster[‡]

Department of Applied Mathematics and Theoretical Physics, University of Cambridge, Cambridge CB3 0WA, United Kingdom

(Received 23 October 2023; accepted 21 March 2024; published 9 April 2024)

We investigate the formation of wrinkling instabilities at the interface between layers of hydrogel and water, which arise to relieve horizontal compressive stresses caused by either differential swelling or confinement. Modelling the gel using a linear-elastic-nonlinear-swelling approach, we determine both a criterion for marginal stability and the growth rates of normal modes. Furthermore, our formalism allows us to understand the influence of differential swelling on the stability of hydrogels brought into contact with water, and we find three distinct phases of the instability. Initially, when only a thin skin layer of gel has swollen, buckles grow rapidly and the gel deforms as an incompressible material. A balance between normal elastic stress and pore pressure selects a wavelength for these buckles that increases with the square root of time. At late times, when the gel approaches a uniformly swollen state, buckles can only grow by differential swelling on much slower timescales determined by solvent transport. At intermediate times, growth is driven by the same fluid transport process as at late times but gradients in fluid pressure in the gel as it swells destabilize the interface, driving faster growth of wrinkles. We also explain why some instabilities can be transient, "healing" as time progresses, while others must remain for all time.

DOI: 10.1103/PhysRevE.109.044602

I. INTRODUCTION

Wrinkling and buckling instabilities are some of the most familiar phenomena observed in the study of soft materials, occurring when there is confinement or other constraints that inhibit the material from expanding. Often instabilities occur due to gradients in the degree of expansion in a direction perpendicular to the surface of the soft material, resulting in the formation of a compressive stress parallel to the surface that can be relieved by the formation of buckles or folds. Familiar examples of this phenomenon include the wrinkling of fruit as it dries and the formation of wrinkles on the surface of human skin as the more compliant lower epidermis and less compliant upper epidermis shrink to different degrees as a result of ageing or damage [1]. More recently, numerous studies have investigated the role played by mechanical wrinkling, folding and creasing during morphogenesis. Key examples include gyrification, the formation of folds and ridges on the surface of the brain during foetal development [2,3], and the shape of fruit and vegetables [4].

The study of wrinkling phenomena began with rubberlike, incompressible solids under mechanical constraints. Perhaps the earliest such work is Euler's classic investigation of a beam under compressive loading, which can snap through to a sinusoidal buckled state on a very short timescale when a critical stress is exceeded [5,6]. Biot [7] studied the purely elastic instability of a half-space of elastic material, showing that wrinkles will form on the surface if the compressive strain parallel to the undeformed interface is greater than a critical value, when deformations of the interface relieve the buildup of elastic potential energy. These deformations are all predicted to form without any volumetric change, and there is no mechanism in Biot's theory to select the size of the wrinkles seen—neither the amplitude nor characteristic lengthscale parallel to the interface.

To address the wavelength-selection problem, Alawiye *et al.* [8] considered a number of two-layer systems with different elastic properties, matching a membranelike deflection of the top layer with an elastic deformation of the anchored base. This problem was also solved in a simpler form by Groenewold [9], who compared their results to experiments carried out with a stiff plate attached to a softer elastic base. Dervaux *et al.* [10] added a surface tension to the interfacial boundary conditions, which stabilizes short-wavelength wrinkles. These methods, taken alongside the stabilizing effect of a fixed base on long-wavelength patterns, select an intermediate wave number that reaches the criterion for marginal stability first, but none discuss the transient state as the instability grows.

As well as being found in incompressible elastic solids, wrinkling instabilities abound in many synthetic or biological examples of soft matter where swelling or drying plays a major role [11]. Superabsorbent polymer hydrogels are a well-studied example of soft materials whose volume can change significantly as a result of swelling or drying. The extremely hydrophilic nature of the polymer chains forming the scaffold of the gel allows them to take on hundreds of times their initial

[*]Present address: Mathematics Institute, University of Warwick, Coventry CV4 7AL, United Kingdom.

[†]joe.webber@warwick.ac.uk; j.webber@damtp.cam.ac.uk

[‡]mgw1@cam.ac.uk

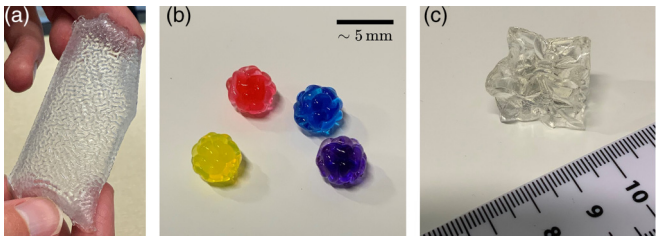

FIG. 1. Three examples of wrinkling in swelling hydrogel materials shortly after contact with water. (a) A thin hydrogel layer (of dry thickness ∼1 mm) anchored to an inextensible plastic base forms a reticulation pattern minutes after immersion in water. (b) Initially spherical hydrogel beads form lobelike wrinkles when swelling commences. (c) A cube of hydrogel forms a crumpled shape. In the latter two of these three cases, further swelling "heals" the wrinkles.

volume in water, and differential swelling and drying can lead to large compressive strains on regions of the gel. It has long been noticed that the surfaces of some swelling gels form a characteristic wrinkling pattern [12], with examples pictured in Fig. 1. Other examples include the reticulation pattern seen on photographic prints [13], formed from wrinkles on the surface of photographic emulsion deposited on the plates during the printing process, and in the "wrinkled pea" texture on the surface of swelling hydrogel beads (Fig. 1(b), and discussed in Bertrand *et al.* [14]).

Though a nuisance in many cases, wrinkling instabilities can be exploited by manufacturers for beneficial purposes. For example, grooves in the surfaces of synthetic materials can be induced to increase biocompatibility of devices for implantation [15], and the presence of fine wrinkled patterns allows for the creation of smart adhesives by increasing the surface area of two materials in contact [16,17].

Many gels are manufactured by covalently anchoring partially dried polymer to a fixed base and adding water [as in Fig. 1(a)], allowing the thin gel layer to swell [18]. It is the formation of wrinkles in this geometry that we consider in the present study. Previous analyses of the wrinkling instability in hydrogels has centered on energy-minimization approaches, finding conditions under which the elastic energy of a hydrogel is decreased by the formation of sinusoidal wrinkles. An important critical parameter is the osmotic pressure, corresponding to the isotropic part of Terzaghi's effective stress, which must exceed a given value for instability [19,20]. Tanaka's approach, which separates the energy of the gel into components due to its bending moment, compression, and stretching, does not predict growth rates but solely deduces criteria for marginal stability. Later studies investigate the wrinkling phenomenon experimentally [18,21] and show that there is a critical strain for instability to arise when gels are attached to a fixed substrate.

A number of distinct behaviors are noted theoretically and experimentally from the earliest studies of the evolution of a wrinkling instability. In all cases, wrinkles form and their wavelengths increase as time progresses, with the wavelength seen to increase initially like the square root of time [21] and to mature like the cube root of time [20]. In some cases, the wrinkles are found to smooth out entirely at late times, or it is seen that the wrinkle pattern evolves to larger wavelengths with sharper creases and folds as nonlinear effects take hold.

More recently, Kang and Huang [22] carried out a linear stability analysis of a uniformly swollen hydrogel layer, using a model based on nonlinear elasticity and nonequilibrium thermodynamics developed by Hong *et al.* [23]. A critical osmotic pressure for exchange of stability can be deduced from this theory but once again there is no discussion of growth rates. It is noted, however, that the first mode to become unstable has infinite wave number, and therefore the theory requires regularization to select a finite most unstable mode. A solution to this selection problem is proposed by Kang and Huang [24], who introduce a surface tension into their model, imposing a normal stress boundary condition described by the Young-Laplace equation. It is then found that both very long and very short wavelengths are stable, selecting a finite "first marginal wave number" as the osmotic pressure is increased to the threshold for instability.

In this paper, we introduce a new approach for finding both the criteria for marginal stability and the growth rates of instability for a finite-thickness layer of uniformly swollen hydrogel brought into contact with water. This allows us to quantify the rate at which wrinkles of a given wave number will grow or shrink and allows us to elucidate the physical processes driving instability. Starting from the foundations of the linear-elastic-nonlinear-swelling model of Webber *et al.* [25,26], we describe the onset of this instability in terms of stresses in the gel and show that, in most cases, wrinkle growth occurs due to swelling and drying of the hydrogel rather than incompressible elastic deformation. This sets a slow diffusive timescale for the growth of wrinkles and describes a mechanism physically distinct from that of pure elasticity. This model is seen to break down at early times, where the mechanism for wrinkle formation is elastic in nature, with the patterned surface forming as the result of an elastic buckling instability. In this case, the system is similar to an elastic bilayer, with the swollen interface anchored to an unswollen base that deforms incompressibly.

Our approach provides an explicit description of the transient base state after hydrogel is brought into contact with water, with the polymer fraction and stress fields determined explicitly, which allows us to carry out a linear stability analysis not only on the uniform state, as in Kang and Huang [22] for example, but also on the transient swelling state, providing a physical explanation for the evolution of the instability observed in the aforementioned experiments and the potential "healing" of wrinkles seen as time progresses.

II. MODELLING SETUP

As a model to investigate wrinkling phenomena, we work in two dimensions and consider a block of hydrogel that is uniformly swollen to a polymer volume fraction ϕ^* and free of deviatoric (shearing) strains, as illustrated in Fig. 2. Initially, the block has thickness a^* and we neglect end effects at the walls, in effect treating them as being an infinite distance apart, while still providing a confining effect. If this block were to be placed in water and left to swell freely, then it would eventually reach the equilibrium polymer volume fraction ϕ_0, and we henceforth scale all polymer fractions with

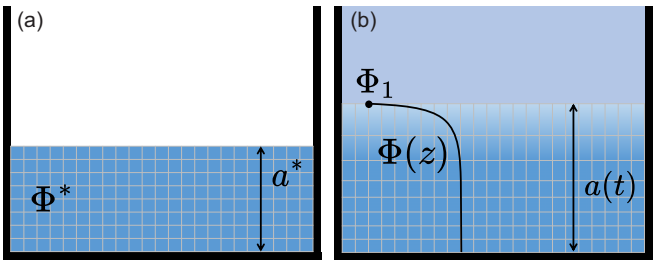

FIG. 2. (a) The isotropic, partially swollen, initial state considered in this model, with uniform polymer fraction Φ^* and a Cauchy strain tensor $\mathbf{e} = (1 - \Phi^{*1/2})\mathbf{I}$ with respect to the fully swollen state $\Phi \equiv 1$. (b) The state of the gel after being brought into contact with water. Notice that horizontal strains do not change but the interface swells to polymer fraction Φ_1.

ϕ_0, writing $\Phi = \phi/\phi_0$. In order for wrinkles to form, however, there needs to be a source of horizontal stress. Therefore, we place this gel block in between horizontal confines and then bring the gel layer into contact with water. As it swells from its initial state $\Phi \equiv \Phi^*$, the side walls provide a horizontal stress that will be relieved by buckling.

A. Constitutive relations

Consider a two-dimensional model with horizontal coordinate x and vertical coordinate z, where the effects of the side walls are encoded by requiring a constant horizontal strain e_{xx}. The gel initially occupies the region $0 \leqslant z \leqslant a^*$, with the water-gel interface being described by $z = a(t)$ at time t. In Webber and Worster [25], the Cauchy strain tensor is found to have an isotropic part due to swelling and drying and a deviatoric part $\boldsymbol{\epsilon}$ due to shear, such that we can write

$$\mathbf{e} = (1 - \Phi^{1/2})\mathbf{I} + \boldsymbol{\epsilon}. \tag{1}$$

Therefore, since the gel is initially isotropically swollen, $\mathsf{e}_{xx} = 1 - \Phi^{*1/2}$. With this condition determined, we now introduce the linear-elastic-nonlinear-swelling theory of Webber and Worster [25] and Webber *et al.* [26]. First, the Cauchy strain tensor $\mathbf{e}$ can be related to displacements $\boldsymbol{\xi} = (\xi,\ \eta)^T$ from the equilibrium (uniformly swollen with $\Phi \equiv 1$) state via

$$\mathbf{e} = \tfrac{1}{2}[\nabla\boldsymbol{\xi} + (\nabla\boldsymbol{\xi})^T] \quad \text{with} \quad \nabla\cdot\boldsymbol{\xi} = 2(1 - \Phi^{1/2}). \tag{2}$$

The constitutive relation linking the stress tensor $\boldsymbol{\sigma}$ to the configuration of the system is also derived in Webber and Worster [25],

$$\boldsymbol{\sigma} = -[p + \Pi(\Phi)]\mathbf{I} + 2\mu_s(\Phi)\boldsymbol{\epsilon}, \tag{3}$$

where p is the pervadic, pore, or pressure [27]; $\Pi(\Phi)$ is the generalized osmotic pressure; and $\mu_s(\Phi)$ is the shear modulus, with these latter two material properties dependent on the polymer fraction. The combination of osmotic and shear contributions to this stress tensor can be together identified with the Terzaghi effective stress in poroelastic models [28].

B. Governing equations and boundary conditions

The equations governing the evolution of the gel in contact with water are

$$\nabla\cdot\boldsymbol{\sigma} = \mathbf{0} \quad \text{and} \tag{4a}$$

$$\frac{\partial\Phi}{\partial t} + \mathbf{q}\cdot\nabla\Phi = \nabla\cdot\left\{\frac{k(\Phi)}{\mu_l}\left[\Phi\frac{\partial\Pi}{\partial\Phi} + \mu_s(\Phi)\Phi^{\frac{1}{2}}\right]\nabla\Phi\right\}, \tag{4b}$$

where $\mathbf{q}$ is the phase-averaged flux, the sum of the interstitial fluid flux and the polymer velocity, and $\nabla\cdot\mathbf{q} = 0$. $k(\Phi)$ is the permeability of the gel, while μ_l is the viscosity of the solvent (in this case water). This is defined in terms of pervadic pressure gradients and deformation of the gel by

$$\mathbf{q} = \Phi^{-1/2}\frac{\partial\boldsymbol{\xi}}{\partial t} - \frac{k(\Phi)}{\mu_l}\nabla p. \tag{5}$$

These equations are to be solved subject to the boundary conditions at the gel-water interface,

$$p = 0, \quad \sigma_{xz} = 0, \quad \text{and} \quad \sigma_{zz} = 0, \tag{6}$$

representing continuity of pervadic pressure, tangential stress, and normal stress, while on the base,

$$\frac{\partial p}{\partial z} = 0, \quad \sigma_{xz} = 0, \quad \mathbf{q}\cdot\hat{\mathbf{z}} = 0, \quad \text{and} \quad \eta = 0, \tag{7}$$

representing no normal flow of water, no shear stress, no net flux of material, and no normal displacement, respectively. For simplicity, we will consider a linear model where $k(\Phi)$ and $\partial\Pi/\partial\Phi$ are both constants, k and K, respectively, and where the shear modulus is polymer fraction independent, $\mu_s(\Phi) = \mu_s$. All the analysis in this paper could be extended straightforwardly to cases where this is not the case, since we expect all three parameters to be polymer fraction dependent in real examples of hydrogels.

C. Computing the base state

In the swelling gel we initially impose horizontal uniformity, so all x derivatives are zero. Hence, $\nabla\cdot\mathbf{q} = 0$ implies that $\partial q_z/\partial z = 0$, where q_z is the vertical component of the total flux. This result can be combined with the observation that the net flux is zero on the bottom boundary (since neither water nor polymer can pass the impermeable base), removing the advective term from Eq. (4b). Then the evolution of polymer fraction field in the layer of gel after contact with water is governed by

$$\frac{\partial\Phi}{\partial t} = \frac{\partial}{\partial z}\left[D(\Phi)\frac{\partial\Phi}{\partial z}\right]; \quad D(\Phi) = \frac{kK}{\mu_l}(\Phi + \mathcal{M}\Phi^{1/2}), \tag{8}$$

where $\mathcal{M} = \mu_s/K$ represents the relative importance of shear stresses compared with osmotic effects. Now the deviatoric strain can be rewritten in terms of the initial polymer fraction Φ^* and the current polymer fraction Φ by noting

$$\mathsf{e}_{xx} = 1 - \Phi^{*1/2} = 1 - \Phi^{1/2} + \epsilon_{xx}, \tag{9}$$

and so $\epsilon_{xx} = -\epsilon_{zz} = \Phi^{1/2} - \Phi^{*1/2}$. The boundary conditions of Eq. (6) combine with this expression for ϵ_{zz} and the constitutive relation of Eq. (3) to set the value of Φ on $z = a(t)$. This interfacial polymer fraction, Φ_1, is determined implicitly

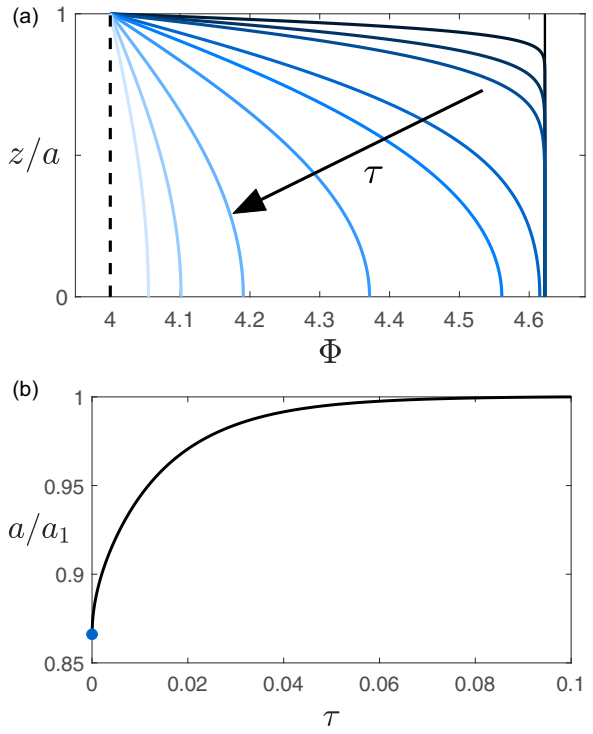

FIG. 3. (a) A plot of the evolution of Φ in time, from Eq. (8), with $\mathcal{M} = 10$ and initial polymer fraction $\Phi^* = 4.6225$ (chosen so that $\Phi_1 = 4$). The arrow points in the direction of increasing time. (b) A plot of the thickness of the gel scaled with the steady-state thickness a_1, showing the diffusive growth of the layer on the swelling timescale, governed by Eq. (13).

by

$$\Phi_1 - 1 = 2\mathcal{M}\left(\Phi^{*1/2} - \Phi_1^{1/2}\right). \tag{10}$$

Now, using the vertical component of Cauchy's momentum Eq. (4a) alongside our expression for ϵ_{zz}, and again invoking horizontal uniformity,

$$\frac{\partial \sigma_{zz}}{\partial z} = 0 \text{ so } \frac{\partial p}{\partial z} = -\frac{D(\Phi)}{\Phi}\frac{\partial \Phi}{\partial z}, \tag{11}$$

and hence the boundary conditions in Eq. (7) imply that $\partial\Phi/\partial z = 0$ on the base. Finally, conservation of polymer shows that

$$\int_0^{a(t)} \Phi \, dz = \Phi^* a^*. \tag{12}$$

This can be differentiated with respect to time and combined with boundary conditions to give a differential equation for $a(t)$,

$$\frac{da}{dt} = -\frac{D(\Phi_1)}{\Phi_1}\frac{\partial \Phi}{\partial z}\bigg|_{z=a(t)}. \tag{13}$$

Figure 3 shows an example set of solutions to these governing equations, showing a polymer fraction that decreases diffusively as water permeates deeper into the gel, approaching the uniform base state where $\Phi \equiv \Phi_1$ through the entire depth, and $a(t) \to a_1$. Throughout this study, we solve this system of equations numerically using the `NDSolve` routine in MATHEMATICA. We can nondimensionalize Eq. (8) through the introduction of the scaled vertical coordinate $\hat{z} = z/a^*$ and the nondimensional time,

$$\tau = \frac{kKt}{\mu_l a^{*2}}. \tag{14}$$

We can also compute the horizontal stress in the swelling gel from the solution to Eq. (8), having seen that the vertical component of Cauchy's momentum equation gives $\sigma_{zz} = 0$ everywhere, so

$$\begin{aligned}\sigma_{xx} &= \sigma_{zz} + 2\mu_s(\epsilon_{xx} - \epsilon_{zz}) = 4\mu_s\epsilon_{xx} \\ &= -4\mu_s(\Phi^{*1/2} - \Phi^{1/2}).\end{aligned} \tag{15}$$

We see that the compressive stress, which can be read from Fig. 3(b) and this expression increases as the gel swells and Φ decreases. At early times, stress is localized near the surface of the gel, while at late times the gel is uniformly stressed horizontally.

D. Early-time similarity solution

At early times $\tau \ll 1$, when the bulk of the gel is yet to swell, the diffusivity D is approximately constant throughout the entire layer, equal to its value at $\Phi = \Phi^*$. Therefore, we let

$$\hat{D} = \frac{\mu_l}{kK}D(\Phi^*) = \Phi^* + \mathcal{M}\Phi^{*1/2}, \tag{16}$$

rendering (8), after nondimensionalization, a linear diffusion equation with diffusivity $\hat{D}$. A further approximation that is valid at early times is to assume that the gel has infinite vertical extent, akin to the confined swelling problem solved in Webber and Worster [25]. Because swelling occurs due to the imbibition of water, it only occurs in a thin boundary layer initially, with the base not felt. Figure 3(a) illustrates that, at early times, the bulk remains unswollen with only a small swollen boundary layer that increases in thickness. Introducing the similarity variable,

$$\chi = \frac{\hat{z} - 1}{2\sqrt{\hat{D}\tau}}, \tag{17}$$

the linearized form of Eq. (8) is found to have the solution

$$\Phi = \Phi^*\left[1 - \left(1 - \frac{\Phi_1}{\Phi^*}\right)\frac{\operatorname{erfc}(-\chi)}{\operatorname{erfc}(-\lambda)}\right], \tag{18}$$

after the application of boundary conditions. This form matches the early-time profiles in Fig. 3(a), with a characteristic diffusive error function shape. The gel thickness is given by

$$a(\tau) = a^*\left(1 + 2\lambda\sqrt{\hat{D}\tau}\right), \tag{19}$$

showing that the swollen boundary layer initially grows with the square root of time. The parameter λ is determined implicitly from

$$\sqrt{\pi}\lambda e^{\lambda^2}\operatorname{erfc}(-\lambda) = \frac{\Phi^*}{\Phi_1} - 1. \tag{20}$$

III. MORPHOLOGICAL STABILITY

With the same modeling framework of the previous section, we can determine the stability of the water-gel interface.

We assume that wrinkle growth occurs faster than changes to the base state and make a "frozen-in-time" approximation, taking a quasistatic base state described by the polymer fraction and pervadic pressure field at $t = t^*$. We perturb the displacement field of gel elements with a perturbation $\varepsilon\tilde{\boldsymbol{\xi}}$, where $\varepsilon \ll 1$ is a small parameter.

Denoting the base state quantities (as derived in Sec. II C) with the subscript $_b$, and the two-dimensional displacement field $\boldsymbol{\xi} = (\xi,\ \eta)^T$, we write

$$\xi = \xi_b(x,\ z;\ t^*) + \varepsilon e^{s(t-t^*)}\tilde{\xi}(z)\sin(\alpha x), \tag{21a}$$

$$\eta = \eta_b(x,\ z;\ t^*) + \varepsilon e^{s(t-t^*)}\tilde{\eta}(z)\cos(\alpha x). \tag{21b}$$

Therefore, the wrinkled interface is described by

$$z = a(t^*) + \varepsilon e^{s(t-t^*)}\tilde{\eta}(a(t^*))\cos(\alpha x) + O(\varepsilon^2), \tag{22}$$

where α is the horizontal wave number and s is the growth rate of the wrinkle, making the usual assumption of linear normal mode analysis that each mode grows or shrinks exponentially in time. These perturbations to the displacement field result in a perturbation to the polymer fraction field,

$$\Phi = \Phi_b(x,\ z;\ t^*) + \varepsilon e^{s(t-t^*)}\tilde{\varphi}(z)\cos(\alpha x). \tag{23}$$

Finally, there may also be a perturbation pervadic pressure,

$$p = p_b(x,\ z;\ t^*) + \varepsilon e^{s(t-t^*)}\tilde{p}(z)\cos(\alpha x). \tag{24}$$

We henceforth abbreviate the base-state quantities, assuming that all are evaluated at time t^* so that $\xi_b(x,\ z) \equiv \xi_b(x,\ z;\ t^*)$.

The order-ε terms in Eq. (2) give a relation between $\tilde{\boldsymbol{\xi}}$ and $\tilde{\varphi}$,

$$\tilde{\varphi} = -\Phi_b^{1/2}(\alpha\tilde{\xi} + \tilde{\eta}'), \tag{25}$$

where $'$ denotes differentiation with respect to z.

A. Momentum balance

Using the definitions in Eqs. (2) and (3) of the Cauchy strain tensor in terms of displacement and the stress tensor, the Cauchy stress tensor can be decomposed into a base state and perturbation part, $\boldsymbol{\sigma} = \boldsymbol{\sigma_b} + \varepsilon e^{s(t-t^*)}\tilde{\boldsymbol{\sigma}}$. It was seen in the previous section that all components of $\boldsymbol{\sigma_b}$ are zero except for $(\sigma_b)_{xx}$, which is given by Eq. (15). The perturbation stress tensor is

$$\tilde{\boldsymbol{\sigma}} = \begin{pmatrix} \left[-(\tilde{p} + K\tilde{\varphi}) + \mu_s\left(\alpha\tilde{\xi} - \frac{\partial\tilde{\eta}}{\partial z}\right)\right]\cos(\alpha x) & \mu_s\left(\frac{\partial\tilde{\xi}}{\partial z} - \alpha\tilde{\eta}\right)\sin(\alpha x) \\ \mu_s\left(\frac{\partial\tilde{\xi}}{\partial z} - \alpha\eta\right)\sin(\alpha x) & \left[-(\tilde{p} + K\tilde{\varphi}) + \mu_s\left(\frac{\partial\tilde{\eta}}{\partial z} - \alpha\tilde{\xi}\right)\right]\cos(\alpha x) \end{pmatrix}. \tag{26}$$

Cauchy's momentum equation in the absence of body forces and neglecting inertial effects implies that $\nabla\cdot\tilde{\boldsymbol{\sigma}} = \mathbf{0}$. Therefore,

$$\mu_s\left(\frac{\partial^2\tilde{\xi}}{\partial z^2} - \alpha^2\tilde{\xi}\right) + \alpha K\tilde{\varphi} + \alpha\tilde{p} = 0, \tag{27a}$$

$$\mu_s\left(\frac{\partial^2\tilde{\eta}}{\partial z^2} - \alpha^2\tilde{\eta}\right) - K\frac{\partial\tilde{\varphi}}{\partial z} - \frac{\partial\tilde{p}}{\partial z} = 0. \tag{27b}$$

It becomes easier to solve the governing equations if we recast in terms of the three variables $\tilde{\eta}$, $\tilde{\varphi}$, and $\tilde{p}$ and can then use Eq. (25) to find $\tilde{\xi}$ given $\tilde{\eta}$ and $\tilde{\varphi}$. Multiplying Eq. (27a) by α and differentiating Eq. (27b) with respect to z, then adding the results, we are left with an equation for $\tilde{\varphi}$,

$$\left(\frac{\partial^2}{\partial z^2} - \alpha^2\right)\left[\frac{D(\Phi_b)}{\Phi_b}\tilde{\varphi} + \tilde{p}\right] = 0. \tag{28}$$

We then encode momentum balance using this equation alongside Eq. (27b). These equations govern the elastic response of the gel to changes in perturbation pervadic and osmotic pressures, but they need to be coupled with another equation linking pressures and displacements arising from the motion of interstitial fluid.

B. Swelling equation

In addition to the mechanical balance above, we also need to consider the swelling-driven dynamics of the perturbations. Swelling is described by Eq. (4b), balancing the rate of change of polymer fraction with advection from the total flux vector and diffusion of water into the gel. As seen above, the equation governing swelling and drying is

$$\frac{\partial\Phi}{\partial t} + \mathbf{q}\cdot\nabla\Phi = \nabla\cdot[D(\Phi)\nabla\Phi]. \tag{29}$$

Letting the perturbation phase-averaged flux be $\tilde{\mathbf{q}} = e^{s(t-t^*)}(\tilde{q}_x\sin(\alpha x),\ \tilde{q}_z\cos(\alpha x))^T$ and working to leading order in the perturbation quantities, this equation becomes

$$\frac{\partial\tilde{\varphi}}{\partial t} + \frac{\partial\Phi_b}{\partial z}\tilde{q}_z = \left(\frac{\partial^2}{\partial z^2} - \alpha^2\right)[D(\Phi_b)\tilde{\varphi}], \tag{30}$$

while Eq. (5) implies that

$$\tilde{q}_z = s\Phi_b^{-1/2}\tilde{\eta} - \frac{1}{2}\Phi_b^{-3/2}\frac{\partial\eta_b}{\partial t}\tilde{\varphi} - \frac{k}{\mu_l}\frac{\partial\tilde{p}}{\partial z}. \tag{31}$$

Since the base state vertical flux $q_z = 0$, the leading-order terms in Eq. (5) give

$$\frac{\partial\eta_b}{\partial t} = \frac{k\Phi_b^{1/2}}{\mu_l}\frac{\partial p_b}{\partial z} = -D(\Phi_b)\Phi_b^{-1/2}\frac{\partial\Phi_b}{\partial z}. \tag{32}$$

We can then combine these two results (31) and (32) to show that

$$\tilde{q}_z = s\Phi_b^{-1/2}\tilde{\eta} + \frac{D(\Phi_b)}{2\Phi_b^2}\frac{\partial\Phi_b}{\partial z}\tilde{\varphi} - \frac{k}{\mu_l}\frac{\partial\tilde{p}}{\partial z}. \tag{33}$$

Taking Eq. (30) and substituting for q_z from Eq. (33) gives

$$s\left(\tilde{\varphi} + \Phi_b^{-1/2}\frac{\partial\Phi_b}{\partial z}\tilde{\eta}\right) - \frac{k}{\mu_l}\frac{\partial\Phi_b}{\partial z}\frac{\partial\tilde{p}}{\partial z} = \left[\frac{\partial^2}{\partial z^2} - \alpha^2 - \frac{1}{2\Phi_b^2}\left(\frac{\partial\Phi_b}{\partial z}\right)^2\right][D(\Phi_b)\tilde{\varphi}], \tag{34}$$

an equation describing the swelling of the gel, a process that governs the growth rate s of instabilities.

C. Boundary conditions

Equations (27b), (28), and (34) together describe a sixth-order system in the three perturbation quantities $\tilde{\eta}$, $\tilde{\varphi}$, and $\tilde{p}$, and we therefore require six boundary conditions to specify the solution uniquely. We start with the boundary conditions on the base of the gel layer (7), where there can be no perturbation vertical displacement ($\tilde{\eta} = 0$) nor a normal interstitial fluid flow across the base, which imposes $\partial\tilde{p}/\partial z = 0$ here.

We also assume no tangential stress σ_{xz} exerted by the gel on the base. Because there is no such stress in the base state (by horizontal uniformity), this condition reduces to requiring $\tilde{\sigma}_{xz} = 0$. Thus, using Eq. (26) and the fact that $\tilde{\eta} = 0$, this reduces to the requirement that $\partial\tilde{\xi}/\partial z = 0$. Differentiating the relation between displacement and $\tilde{\varphi}$ of Eq. (25) and using the fact that $\partial\Phi_b/\partial z = 0$ on $z = 0$ and the governing Eq. (27b) for $\partial^2\tilde{\eta}/\partial z^2$, this can be transformed into a condition $\partial\tilde{\varphi}/\partial z = 0$, so the boundary conditions to be applied on $z = 0$ are

$$\tilde{\eta} = \frac{\partial\tilde{\varphi}}{\partial z} = \frac{\partial\tilde{p}}{\partial z} = 0. \tag{35}$$

On the interface between gel and water, the boundary conditions of Eq. (6) imply that we require continuity of stress and pervadic pressure. Assuming, without loss of generality, that the pervadic pressure and the stress tensor are both zero in the fluid overlying the gel, the boundary condition on the pervadic pressure is

$$p = p_b + \varepsilon e^{s(t-t^*)}\tilde{p}\cos(\alpha x) = 0 \tag{36}$$

at $z = a(t^*) + \varepsilon e^{s(t-t^*)}\tilde{\eta}\cos(\alpha x)$, which linearizes to

$$\tilde{p} + \frac{\partial p_b}{\partial z}\tilde{\eta} = 0 \quad \text{at } z = a(t^*), \tag{37}$$

since $p_b[a(t^*)] = 0$ by continuity. An expression for $\partial p_b/\partial z$ is shown in Eq. (11), and so

$$\tilde{p} = \frac{D(\Phi_1)}{\Phi_1}\frac{\partial\Phi_b}{\partial z}\tilde{\eta} \quad \text{at } z = a(t^*). \tag{38}$$

In order to impose normal and tangential stress boundary conditions, we first calculate the normal vector to the deformed interface, described, at leading order, by

$$\begin{aligned}\mathbf{n} &= \nabla\left(z - \left\{a(t^*) + \varepsilon e^{s(t-t^*)}\tilde{\eta}[a(t^*)]\cos(\alpha x)\right\}\right)\\ &= \begin{pmatrix}\varepsilon\alpha e^{s(t-t^*)}\tilde{\eta}[a(t^*)]\sin(\alpha x)\\ 1\end{pmatrix}.\end{aligned} \tag{39}$$

Hence, the total surface stress $\mathbf{\Sigma} = [\boldsymbol{\sigma_b} + \varepsilon e^{s(t-t^*)}\tilde{\boldsymbol{\sigma}}]\cdot\mathbf{n}$ is

$$\begin{pmatrix}\left[\mu_s\left(\frac{\partial\tilde{\xi}}{\partial z} - \alpha\tilde{\eta}\right) - 2K\alpha\tilde{\eta}(\Phi_1 - 1)\right]\sin(\alpha x)\\ \left[\left(K\Phi_1^{\frac{1}{2}} - \mu_s\right)\alpha\tilde{\xi} + \left(K\Phi_1^{\frac{1}{2}} + \mu_s\right)\frac{\partial\tilde{\eta}}{\partial z} - \tilde{p}\right]\cos(\alpha x)\end{pmatrix}, \tag{40}$$

up to and including terms of order ε, with all functions evaluated at $z = a(t^*)$. Since continuity of normal and tangential stress is equivalent to the requirement that $\mathbf{\Sigma} = \mathbf{0}$, this provides another two boundary conditions for the stability calculation and thus closes the system. Differentiating Eq. (25) to substitute for $\partial\tilde{\xi}/\partial z$ and using Eq. (27b), the tangential stress condition on $z = a(t)$ becomes

$$\frac{\partial}{\partial z}\left[\frac{D(\Phi_b)}{\Phi_b}\tilde{\varphi} + \tilde{p}\right] + 2[K(\Phi_1 - 1) + \mu_s]\alpha^2\tilde{\eta} = 0. \tag{41}$$

The normal stress condition can also be restated, using Eq. (38) to substitute for $\tilde{p}$, as

$$2\mu_s\frac{\partial\tilde{\eta}}{\partial z} = \left(K - \mu_s\Phi_1^{-1/2}\right)\tilde{\varphi} - \frac{D(\Phi_1)}{\Phi_1}\frac{\partial\Phi_b}{\partial z}\tilde{\eta}. \tag{42}$$

D. Nondimensionalization

Equations (27b), (28), and (34) can be solved alongside boundary conditions provided in Eqs. (35), (38), (41), and (42) in order to find the unknown growth rate s given a wave number α, material properties, as well as the base swelling state (i.e., the gel thickness and polymer fraction field). Since our stability analysis makes a "frozen-in-time" approximation, we scale all lengths with the thickness of the gel $a(t^*)$ and introduce the variable $y = z/a(t^*)$ so that our spatial domain becomes $0 \leqslant y \leqslant 1$. To summarize, let

$$\bar{\alpha} = \alpha a(t^*); \quad \bar{\eta} = \frac{\tilde{\eta}}{a(t^*)}. \tag{43}$$

Furthermore, we scale all pressures with the osmotic modulus K and let s scale with a diffusive timescale [as also seen in Eq. (14)],

$$\bar{p} = \frac{\tilde{p}}{K}; \quad \bar{p}_b = \frac{p_b}{K}; \quad \bar{s} = \frac{\mu_l a^2 s}{kK}; \quad \bar{D}(\Phi) = \frac{\mu_l D(\Phi)}{kK}, \tag{44}$$

where $a = a(t^*)$ for brevity. Then, dropping the bar markers and letting $\Phi_b = \Phi$ for clarity, the nondimensional system of equations and boundary conditions becomes

$$\mathcal{M}\left(\frac{\partial^2}{\partial y^2} - \alpha^2\right)\eta = \frac{\partial}{\partial y}(p + \varphi), \tag{45a}$$

$$\left(\frac{\partial^2}{\partial y^2} - \alpha^2\right)\left[\frac{D(\Phi)}{\Phi}\varphi + p\right] = 0, \tag{45b}$$

$$s\left(\varphi + \Phi^{-\frac{1}{2}}\frac{\partial\Phi}{\partial y}\eta\right) - \frac{\partial\Phi}{\partial y}\frac{\partial p}{\partial y} = \left[\frac{\partial^2}{\partial y^2} - \alpha^2 - \frac{1}{2\Phi^2}\left(\frac{\partial\Phi}{\partial y}\right)^2\right][D(\Phi)\varphi], \tag{45c}$$

$$\left.\begin{aligned}\eta &= \tfrac{\partial\varphi}{\partial y} = 0,\\ \tfrac{\partial p}{\partial y} &= 0.\end{aligned}\right\} \quad \text{on } y = 0. \tag{45d}$$

$$\left.\begin{aligned} p &= \tfrac{D(\Phi_1)}{\Phi_1}\tfrac{\partial \Phi}{\partial y}\eta, \\ \tfrac{\partial}{\partial y}\left[\tfrac{D(\Phi)}{\Phi}\varphi + p\right] + 2(\mathcal{M} + \Phi_1 - 1)\alpha^2\eta &= 0, \\ 2\mathcal{M}\tfrac{\partial \eta}{\partial y} &= \left(1 - \mathcal{M}\Phi_1^{-1/2}\right)\varphi - \tfrac{D(\Phi_1)}{\Phi_1}\tfrac{\partial \Phi}{\partial y}\eta. \end{aligned}\right\} \quad \text{on } y = 1. \tag{45e}$$

In order to solve these equations numerically, we can convert them into a matrix form (see Appendix B) and seek solutions for the growth rate s as a function of wave number α by using the boundary conditions to formulate a solvability criterion.

IV. GEL LAYERS WITH UNIFORM POLYMER FRACTION

Before considering the effect of the transient swelling state on the instability, we start by solving the simpler problem in which a gel has swollen to a uniform polymer fraction $\Phi \equiv \Phi_1$, and there are therefore no base state pervadic pressure gradients—no interstitial fluid is flowing through the polymer scaffold. Therefore, $D(\Phi)$ is a constant, D, and $\partial\Phi/\partial y \equiv 0$.

A. Criteria for marginal stability

We start by considering the criteria for marginal stability, where $s = 0$ and perturbations neither grow nor shrink, allowing us to identify critical values of the material parameters beyond which instability is seen. In this case Eqs. (45b) and (45c) combine to show

$$\left(\frac{\partial^2}{\partial y^2} - \alpha^2\right)p = 0 \quad \text{with} \quad \left.\frac{\partial p}{\partial y}\right|_{y=0} = p(1) = 0, \tag{46}$$

from boundary conditions (45d) and (45e). The only solution to this system is $p \equiv 0$, and there is thus no perturbation pervadic pressure field, and hence no perturbation fluid flow. This is to be expected, since fluid flows lead to swelling and shrinkage, which would lead to growth or decay of the wrinkles. Solving the remaining equations for this marginally stable incompressible mode, as outlined in Appendix B, and applying the boundary conditions gives the solvability criterion for marginal stability,

$$\mathcal{M}\left(1 + \Phi_1^{\frac{1}{2}} - \Phi_1\right)\sinh(2\alpha) + 2\Phi_1^{\frac{1}{2}}(\mathcal{M} + \Phi_1 - 1)\alpha = 0. \tag{47}$$

The plots in Fig. 4 illustrate that an instability is first triggered at infinitely small wavelength, $\alpha \to \infty$. Taking the limit $\alpha \to \infty$ of Eq. (47), it can be seen that the critical value of Φ_1 to reach marginal stability is given by $\Phi_{\text{crit}} = (3 + \sqrt{5})/2$.

It is also clear that there is no nontrivial marginally stable mode when $\mathcal{M} = 0$, where the compressive strain will not lead to a deviatoric stress, so buckling is not necessary to relieve stresses. Notice also that the critical value of Φ_1 for an instability of zero wave number ($\alpha = 0$) to be triggered is only finite for $\mathcal{M} > 3 + 2\sqrt{2} \approx 5.83$. In general, increasing $\mathcal{M}$ results in a less stable situation, with a lower value of Φ_1 needed to trigger an instability, as the same compressive strain results in a much larger compressive stress (to relieve through the formation of wrinkles) in this case.

Though our equations specify a critical steady-state polymer fraction for an instability, this is a dependent variable and it is more instructive to view the threshold for instability in terms of the compressive stress or strain exerted by the side walls. Since we know that instability is triggered once Φ_1 exceeds Φ_{crit}, our marginal stability criterion can be transformed into a condition on horizontal compressive stress using Eqs. (10) and (15),

$$\sigma_{xx} \leqslant -2K(\Phi_{\text{crit}} - 1) \quad \text{so} \quad \sigma_{xx} \leqslant -K(\sqrt{5} - 1). \tag{48}$$

We can also convert the criterion on Φ_1 to a criterion on e_{xx} using the definition of Φ_1 in terms of Φ^* and the fact that $\mathsf{e}_{xx} = 1 - \Phi^{*1/2}$. Results are plotted in Fig. 5, showing that very large compressive strains are needed to trigger an instability as $\mathcal{M} \to 0$, since large strains are needed to achieve the critical stress when the material's shear modulus is low.

Previous studies have expressed the criterion for marginal stability in a number of different ways. Tanaka *et al.* [19] deduce a critical osmotic modulus in terms of two elastic constants for the hydrogel, assuming that all deformations are in the vertical direction. On the other hand, Trujillo *et al.* [18] reference the predictions of Biot's theory [7] that instability would be expected above a critical compressive strain of around 0.33 and find the same result experimentally under equibiaxial compression (i.e., the same compression in both orthogonal directions parallel to the gel interface). Kang and

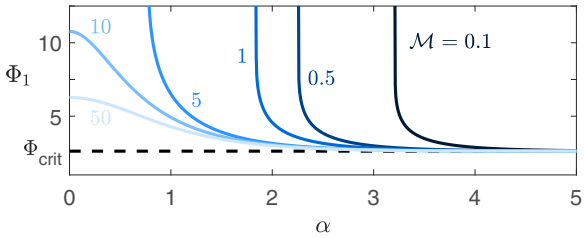

FIG. 4. Plots of the marginally stable value of Φ_1, determined implicitly in Eq. (47), at which wrinkles neither grow nor shrink, against wave number α, showing that instability is triggered first at infinite wave number α, with, in general, stabilization for small α and a critical value $\Phi_1 \geqslant \Phi_{\text{crit}} = (3 + \sqrt{5})/2$ for instability.

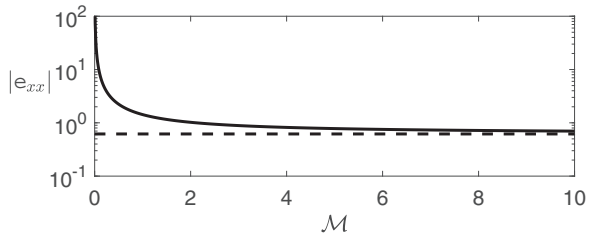

FIG. 5. Plots of the critical compressive strain $-\mathsf{e}_{xx}$ to trigger an instability of any wave number [i.e., to have $\Phi_1 \geqslant (3 + \sqrt{5})/2$] in the uniformly swollen steady state for different values of $\mathcal{M}$. The dashed line shows the large-$\mathcal{M}$ limit for e_{xx}, equal to $(\sqrt{5} - 1)/2 \approx 0.618$.

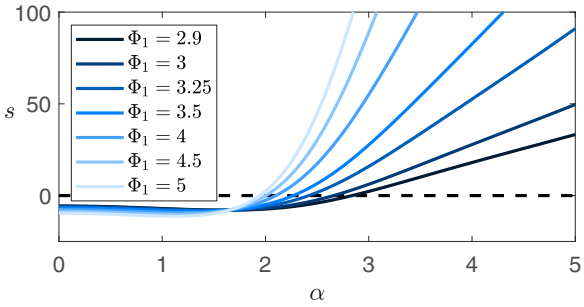

FIG. 6. Plots of the dispersion relation (49) for the growth rate s as a function of wave number α and polymer fraction Φ_1 when $\mathcal{M} = 1$, showing faster growth for larger Φ_1 or α.

Huang [22] deduce a critical swelling ratio λ (related to the thickness of the gel relative to its "dry" state) that they find depends on material properties and can convert to a critical linear strain of around 0.33.

Though the predictions of our model cannot be compared directly with any of these earlier approaches due to our modeling being purely two dimensional, qualitatively our results agree with those of Kang and Huang [22], with a higher threshold for instability as $\alpha \to 0$ and a plateau with an approximately constant threshold as $\alpha \to \infty$.

B. Calculating growth rates

As discussed above, a number of studies compare the wrinkling instability to the elastic instability of a half-space studied by Biot [7,18,22], where buckles form *via* an incompressible elastic deformation with no volumetric change. In these studies, a marginally stable solution is found but no mechanism for growth or shrinkage of the wrinkles is proposed. However, it is clear that the mechanism underlying the growth of wrinkles in our model is entirely different. Equation (45c) shows that, when $\partial\Phi/\partial y = 0$, the growth rate s only appears multiplied by φ and so a volumetric change is required, which, for a hydrogel, must correspond to swelling and drying and therefore some flow. It is this process that sets the growth rate for wrinkles in the uniformly swollen case.

The perturbation Eqs. (45) with $\Phi \equiv \Phi_1$ can be solved analytically for the perturbation eigenfunctions (as detailed in Appendices A and B) to yield the implicit dispersion relation,

$$\frac{\mathcal{M}s}{2\alpha}\sinh(2\alpha) + (\mathcal{M}+\Phi_1-1)\left[s+\mathcal{M}\Phi_1^{\frac{1}{2}}\alpha\sinh(2\alpha)\right] = 2\mathcal{M}\Phi_1^{\frac{1}{2}}(\mathcal{M}+\Phi_1-1)\sqrt{\alpha^2+\frac{s}{D}} \times \cosh^2(\alpha)\tanh\left(\sqrt{\alpha^2+\frac{s}{D}}\right). \tag{49}$$

The dependence of growth rate s on α and Φ_1 is illustrated in Fig. 6. The large values away from marginal conditions show that the growth rate is significantly faster than the slower swelling timescale at which the gel reaches its uniformly swollen state. Later, when considering the transient swelling problem, this justifies our use of the frozen-in-time approximation. In the limit $\alpha \gg 1$, Eq. (49) implies that

$$s \approx \frac{4\Phi_1^{1/2}(1-\mathcal{M}-\Phi_1)\left(1+\Phi_1^{1/2}-\Phi_1\right)}{\mathcal{M}+\Phi_1^{1/2}}\alpha^2, \tag{50}$$

so the growth rate is approximately quadratic in the wave number when the wrinkles have a much shorter wavelength than the depth of the layer (recall that α is scaled with a_1 in the uniformly swollen case). On the other hand, we find stabilization as $\alpha \to 0$, with s approaching a finite negative value.

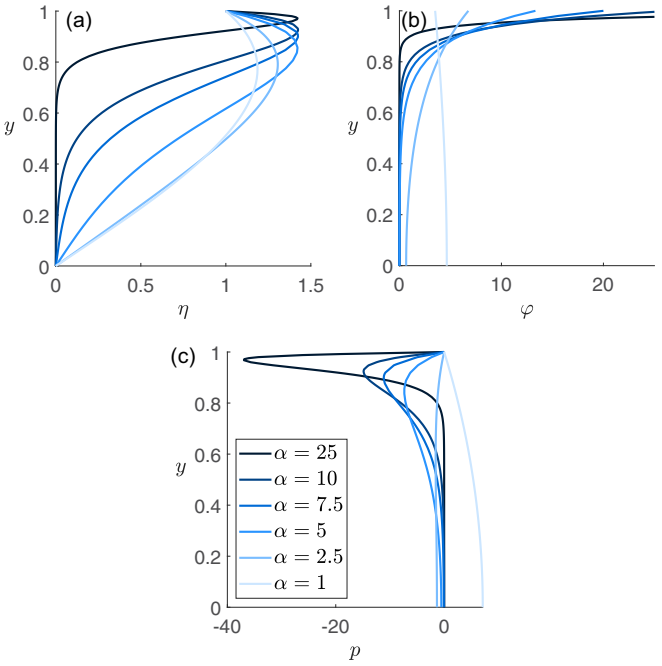

FIG. 7. Plots of the perturbation eigenfunctions, normalized by the value of η at $y = 1$, for a variety of wave numbers when $\mathcal{M} = 1$ and $\Phi_1 = 4$, as derived in Eq. (A3). In these examples, all but $\alpha = 1$ are unstable. Notice that $p_y < 0$ at $y = 1$ in all the unstable cases and $p_y > 0$ in the stable case. Also note the decreasing decay lengthscale as α increases.

C. Perturbation eigenfunctions

As well as deducing the dispersion relation for $s(\mathcal{M}, \Phi_1, \alpha)$, solving Eqs. (45) gives the form of the perturbation eigenfunctions η, φ, and p at any given wave number. Example eigenfunctions, normalized by the value of η on the interface, are shown in Fig. 7, illustrating the decay of perturbation quantities away from the interface. Perhaps the most instructive of these is the pervadic pressure eigenfunctions, since the interstitial flow is driven from regions of high pervadic pressure to lower pressures *via* Darcy's law [27].

Figure 8 illustrates the interstitial flow field in both unstable and stable cases, showing the mechanisms that drive the growth and shrinkage of wrinkles. If $\partial p/\partial y < 0$ for all values of y, then a flow is driven from the gel into the bulk fluid above; i.e., wrinkles shrink by expelling water from swollen regions and drawing it into shrunken troughs and the gel is stable. When unstable, however, $\partial p/\partial y > 0$ at the interface,

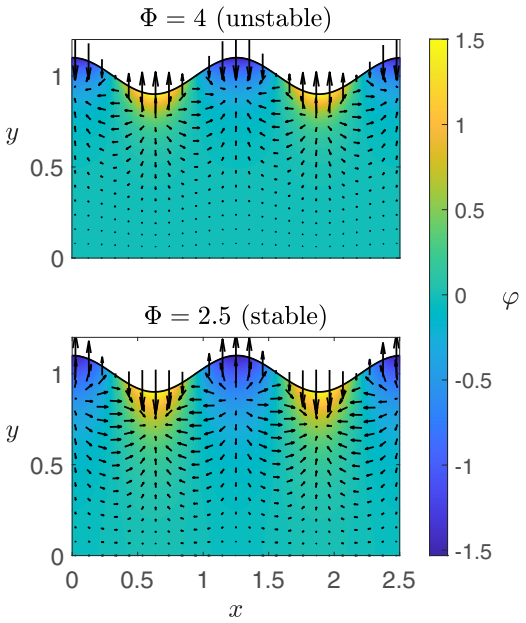

FIG. 8. Contour plots of the perturbation polymer fraction field $\tilde{\varphi}$ (A3a) alongside arrows indicating the direction of the interstitial fluid flow in each case, underlining the growth or shrinkage mechanism. When the polymer fraction is low, fluid is driven out of peaks and into troughs, stabilizing the interface, while the opposite happens in unstable cases. In both cases, $\mathcal{M} = 1$ and $\alpha = 5$.

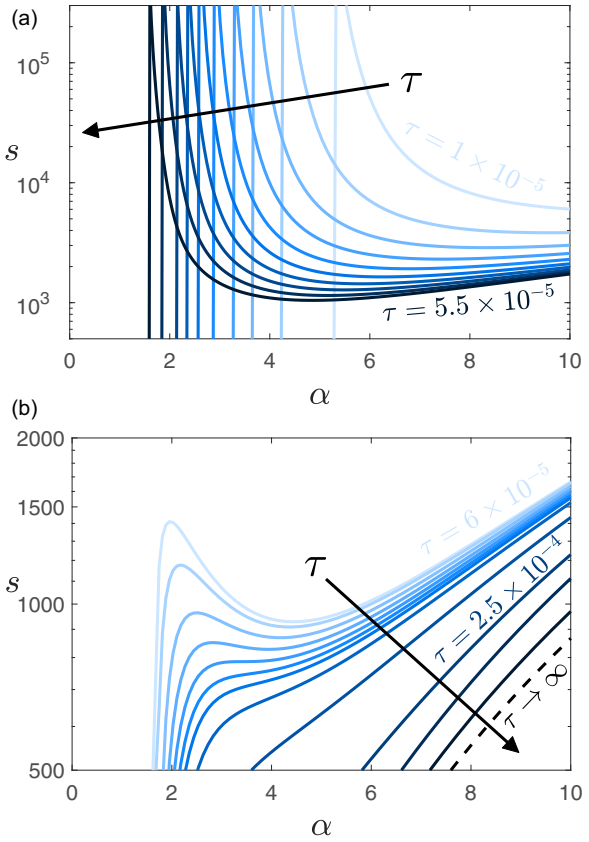

FIG. 9. Plots of the dispersion relation for a swelling gel at various times τ when $\mathcal{M} = 10$ and $\Phi^* = 4.6225$ (and thus $\Phi_1 = 4$), with a logarithmic scale for s. (a) The dispersion relation for early times, showing a distinct peak at a finite wave number α^*. (b) The peaks seen at early times disappear beyond $\tau \approx 5.5 \times 10^{-5}$ and the growth rates decrease, approaching the steady-state value derived in Sec. IV with $\Phi_1 \equiv 4$.

driving a flow from the overlying fluid into peaks (and out of troughs), but $\partial p/\partial y < 0$ deeper in the gel, driving flow from the bulk into peaks and out of troughs, exaggerating their growth with water from below as well.

V. BUCKLING INSTABILITY AT EARLY TIMES

Since instabilities have been seen to grow much faster than the planar interface of hydrogel swells, we make a quasistatic approximation and can solve the full set of governing equations (45) with numerical solutions for the base state from Eqs. (8) in order to find the dispersion relation $s(\alpha, \tau)$ at any given nondimensional time τ. Some representative results of this are shown in Figs. 9 and 10. In contrast with Fig. 6, we see further destabilization at early times, with growth rates tending to infinity at specific wave numbers $\alpha^*(\tau)$, and growth rates being larger than in the uniformly swollen case for all wave numbers.

Given that we have not included inertia in the force-balance equation, these infinite growth rates indicate a purely elastic buckling instability akin to the buckling of an Euler beam [6], which grow on the fast elastic timescale governed by inertia alone. Instead of the gel swelling and drying to form a new state, it deforms incompressibly, just like a pure elastic material, to reach the new patterned state.

The steady base state studied in Sec. IV has a uniform compression throughout the depth of the gel. During transient swelling, however, as illustrated in Fig. 3(a) and Eq. (15), compressive stresses are confined to a boundary layer near the surface of the gel, leading to qualitatively different behavior. In addition to the different mechanical constraints on the hydrogel due to differential swelling, the presence of gradients in the polymer fraction field modifies the pervadic pressure boundary condition. As a gel swells, its interface is presumed to swell instantaneously to the interfacial polymer fraction Φ_1, with the bulk of the gel having a higher polymer fraction. Therefore, $\partial\Phi/\partial y < 0$ at $y = 1$, and the interfacial boundary condition (45e) on the pervadic pressure becomes

$$p(1) = \frac{D(\Phi_1)}{\Phi_1} \left.\frac{\partial \Phi}{\partial y}\right|_{y=1} \eta(1). \tag{51}$$

Therefore, since $\partial\Phi/\partial y < 0$, peaks on the wrinkled interface correspond to minima in the perturbation pressure and troughs to maxima, driving interstitial flow into peaks and accelerating the growth of any instabilities.

In this section, we investigate the rapid growth seen at specific wave numbers α^* which is expected to dominate the dynamics of the interface at early times. Figure 11 shows the wave number at which this peak occurs and how it depends on time, illustrating how $\alpha^* \sim \tau^{-1/2}$ at early times, with the wave number of the instability decreasing down to around $\alpha \approx 1$ before this mechanism no longer plays a part. Figure 9(b) shows that, above a certain critical time $\tau = \tau_{\text{buckle}}$ (for this choice of parameters $\approx 5.5 \times 10^{-5}$), the buckling mechanism no longer plays a role, and the dispersion relation approaches

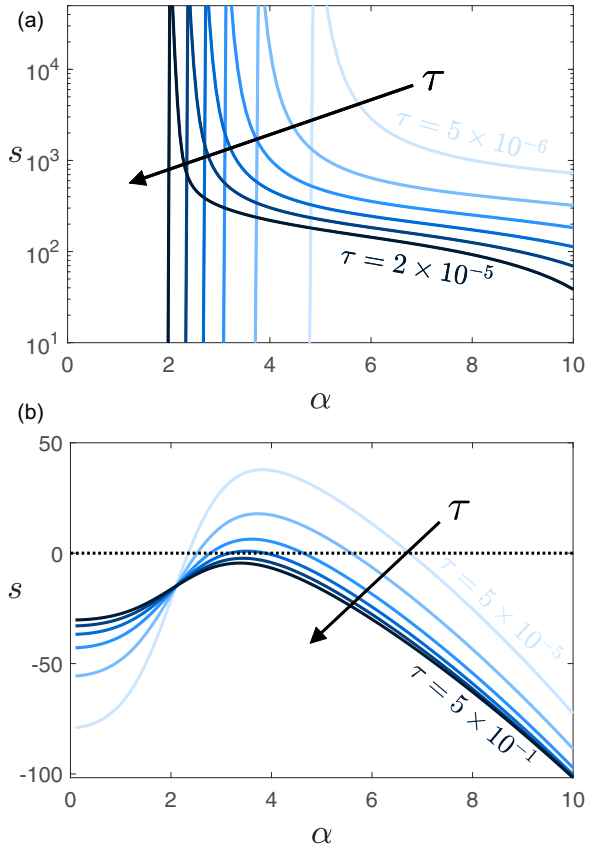

FIG. 10. Plots of the dispersion relation at early times (a) and later times (b) when $\Phi^* = 2.75$ and $\mathcal{M} = 10$. In this case, $\Phi_1 < \Phi_{\text{crit}}$ and thus the final steady state is stable to perturbations of all wave numbers. However, as $\tau \to 0$, some wave numbers are unstable. Note the logarithmic scale in (a) and the linear scale in (b).

the steady-state value from Sec. IV as the gel swells to a state where $\Phi \equiv \Phi_1$.

A. Healing of instabilities

Since growth rates for a given wave number decrease in time as the gel approaches a steady state and that it is clear that there is a different elastic mechanism at play when only a boundary layer of gel is swollen, it is reasonable to assume

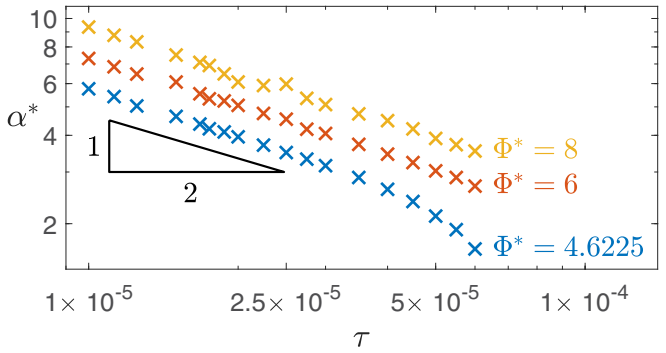

FIG. 11. Plots of the most unstable mode α^* where the growth rate approaches infinity at early times, with $\mathcal{M} = 10$, for different values of Φ^*, showing that $\alpha^* \propto \tau^{-1/2}$ at early times.

that gels where $\Phi_1 < \Phi_{\text{crit}}$ may be unstable at early times before becoming stable as these different mechanisms become less influential.

This is seen to be the case in the plots of Fig. 10, where, at early times, we see qualitatively similar behavior to the early-time peaks seen in cases where $\Phi_1 > \Phi_{\text{crit}}$, but at later times it is apparent that $s < 0$ for all wave numbers. There is an intermediate regime where a band of wave numbers remain unstable but both short- and long-wavelength wrinkles are suppressed, as seen in Fig. 10(b).

We propose that this can explain the transient nature of wrinkled interfacial patterns in some cases, where wrinkles form but are no longer apparent at later times. Though explaining the smoothing and healing of the wrinkles themselves would require a nonlinear analysis, these results show that there are some situations in which linear instability is only present at the earliest stages of swelling.

B. Elastic buckling

The full numerical results of Fig. 9(a) suggest the presence of an elastic buckling instability at very early times when only a thin layer of gel at the gel-water interface has swollen to $\Phi = \Phi_1$. This instability occurs only for one wave number α^*, and we plot the time evolution of this wave number in Fig. 11. The rapid growth of this instability suggests that the underlying mechanism cannot involve swelling or drying—there must be a different, faster, growth mechanism. The lack of swelling and drying implies that there can be no gradients in perturbation pervadic pressure p (as these would drive flow) and we relax the requirement of continuity of tangential stress at $y = 1$, owing to the presence of a swollen "skin" which is free to be sheared. Furthermore, at these early times, the bulk of the gel is assumed to remain at its initial polymer fraction Φ^*, so Eqs. (45) become

$$\mathcal{M}\left(\frac{\partial^2}{\partial y^2} - \alpha^2\right)\eta = 0, \tag{52a}$$

$$\eta = 0 \quad \text{on } y = 0, \tag{52b}$$

$$2\mathcal{M}\frac{\partial \eta}{\partial y} = -\frac{D(\Phi^*)}{\Phi^*}\Phi_y \eta \quad \text{on } y = 1. \tag{52c}$$

where Φ_y denotes the value of $\partial\Phi/\partial y$ at $y = 1$. Since the value of η at $y = 1$ is a free parameter equal to the amplitude of the wrinkles, the equation for η is overdetermined with two boundary conditions. Therefore, a single value of α is selected by the normal stress boundary condition, and this corresponds to the wave number α^* where s was seen to approach infinity in the numerical solutions. Equation (52a) can be solved straightforwardly alongside boundary condition (52b) to find that

$$\frac{\eta}{\eta(1)} = \frac{\sinh(\alpha^* y)}{\sinh \alpha^*}. \tag{53}$$

Then, using this result, the normal stress matching condition implies that

$$\alpha^* = -\frac{D(\Phi^*)\Phi_y}{2\mathcal{M}\Phi^*}\tanh \alpha^*. \tag{54}$$

This result can be reinterpreted in terms of the thickness of the swollen boundary layer Δ at the gel-water interface.

Noting that

$$\Phi_y \approx \frac{\Phi_1 - \Phi^*}{\Delta/a(\tau)} \quad \text{whence} \quad \Delta \approx -\frac{\Phi^* - \Phi_1}{\Phi_y}\, a(\tau), \tag{55}$$

we define $\delta = \Delta/a(\tau)$ as the fraction of the gel thickness occupied by the swollen boundary layer. Hence Eq. (54) can be restated as

$$\alpha^* = \frac{D(\Phi^*)}{2\mathcal{M}\delta}\left(1 - \frac{\Phi_1}{\Phi^*}\right)\tanh\alpha^*. \tag{56}$$

At the very earliest times, when the boundary layer fraction $\delta \ll 1$, it is found that

$$\alpha^*\delta \approx \frac{D(\Phi^*)}{2\mathcal{M}}\left(1 - \frac{\Phi_1}{\Phi^*}\right), \tag{57}$$

and therefore the wavelength of the wrinkles is set by the thickness of the boundary layer. There is one solution to Eq. (56) provided that δ is sufficiently small for a solution to exist, but once δ exceeds a critical value δ_c, given by

$$\delta_c = \frac{D(\Phi^*)}{2\mathcal{M}}\left(1 - \frac{\Phi_1}{\Phi^*}\right), \tag{58}$$

there is no longer a solution α^* and no elastic buckling is possible. It can be verified that $\delta_c < 1$ except in cases where both $\mathcal{M}$ is small and there is a large contrast between Φ^* and Φ_1, when the founding assumption that ϵ_{zz} is small no longer holds, and so our modeling is not expected to be valid.

C. Physical mechanism for the buckling instability

In order to understand the physical processes that lead to the onset of the buckling instability, we model the hydrogel as an incompressible elastic bulk topped by a flexible plate representing the swollen layer, with $\delta \ll 1$ at early times. In this model, we are effectively seeking the criterion for buckling of an Euler beam tethered along its length to an incompressible elastic foundation. The load on this plate comes from the normal stress exerted on its upper and lower surfaces, with the assumption that p balances osmotic pressures in the initially unstressed bulk, so the net load (in the vertical direction) on the membrane, $\mathcal{Q}$, is

$$\begin{aligned}\mathcal{Q} &= [\sigma_{zz}]_{y=1-\delta}^{y=1} = -p(1)\cos(\alpha x) - \sigma_{zz}^{\text{bulk}}\big|_{y=1-\delta} \\ &= -\frac{D(\Phi^*)\Phi_y}{\Phi^*}\eta(1)\cos(\alpha x) - \sigma_{zz}^{\text{bulk}}\big|_{y=1-\delta},\end{aligned} \tag{59}$$

using the interfacial boundary condition for p. The shape of the plate is described by $\eta = A\cos(\alpha x)$, and this must match the vertical displacement $\eta(1)$ since the two layers remain attached. Within the bulk, we assume an incompressible deformation, so there exists a stream function ψ such that

$$\xi = \frac{\partial\psi}{\partial y} \quad \text{and} \quad \eta = -\frac{\partial\psi}{\partial x} \quad \text{with} \quad \nabla(\nabla^2\psi) = \mathbf{0}, \tag{60}$$

the latter equation arising from Cauchy's momentum equation in the absence of bulk pressures. Matching with the interfacial shape, we know that $\psi = \hat{\psi}(y)\sin(\alpha x)$, with boundary conditions

$$\hat{\psi} = 0 \quad \text{on} \quad y = 0 \quad \text{and} \quad \alpha\hat{\psi} = -A \quad \text{on } y = 1 - \delta. \tag{61}$$

The most general solution for $\hat{\psi}$, from Eq. (60) and the form we have chosen for x dependence, is

$$\hat{\psi} = a_1\cosh(\alpha y) + a_2\sinh(\alpha y). \tag{62}$$

Thus,

$$\hat{\psi} = -\frac{A\sinh(\alpha y)}{\alpha\sinh[\alpha(1-\delta)]} \quad \text{and} \quad \eta = -\alpha\hat{\psi}(y)\cos(\alpha x). \tag{63}$$

Furthermore, since $\sigma_{zz}^{\text{bulk}} = 2\mathcal{M}\partial\eta/\partial y$ in the incompressible case, Eq. (59) finally becomes

$$\mathcal{Q} = -A\left\{\frac{D(\Phi^*)\Phi_y}{\Phi^*} + \frac{2\mathcal{M}\alpha}{\tanh[\alpha(1-\delta)]}\right\}\cos(\alpha x). \tag{64}$$

The deflection arising from applied stresses is described by the Föppl-von Kármán equation, since the plate is thin at early times,

$$\begin{aligned}&\frac{E\delta^3}{12(1-\nu^2)}\alpha^4 - 4\mathcal{M}\left(\Phi^{*1/2} - \Phi_1^{1/2}\right)\delta\alpha^2 \\ &\quad = -\left\{\frac{D(\Phi^*)\Phi_y}{\Phi^*} + \frac{2\mathcal{M}\alpha}{\tanh[\alpha(1-\delta)]}\right\}\cos(\alpha x).\end{aligned} \tag{65}$$

The first term, with its dependence on the elastic modulus E, Poisson's ratio ν, and layer thickness δ, represents the effect of the bending moment on the membrane. The second term incorporates the effect of prestressing, with the horizontal compressive stress due to swelling derived in Eq. (15). Finally, the right-hand side represents the balance between the interfacial pervadic pressure and the restraining force from the elastic bulk. Since δ is assumed small, we consider only the leading-order contributions, setting the right-hand side $\mathcal{Q}$ of Eq. (65) to zero, which gives exactly the same equation for α^* as Eq. (54).

In the transient swelling state, there is more compressive stress at the interface than in the bulk, owing to greater degrees of swelling near the gel-water interface. These stresses are balanced by a pervadic pressure field, with higher pressures at the interface acting against these deviatoric elastic stresses, and it is this nonuniform pervadic pressure distribution in the base state that leads to the boundary condition on the perturbation pervadic pressure. Thus, the interfacial pressure term in Eq. (59) arises directly from compression at the interface and is balanced by the anchoring force. Thus, the instability is driven entirely by a balance between these compressive stresses arising from swelling and anchoring from the base.

As was seen above, there is a critical value of δ, δ_c, beyond which the stabilizing influence of the fixed base is too strong for elastic buckling to occur, and this value is defined by Eq. (58). Viewing the early-time buckling instability as an elastic beam anchored to a surface shows more clearly, however, that the stabilization of this mechanism arises from the anchored base. There is always a nonzero solution α to $\mathcal{Q} = 0$ when $\Phi_y \neq 0$, so buckling instabilities can occur at all finite times. It is only the growing influence of the anchored base that stabilizes this mechanism.

D. Transition between early and late regimes

The above reasoning explains the location of the peak in Figs. 9(a) and 10(a), as well as the mechanism by which instabilities arise in these very specific cases. However, we still have yet to explain the growth rates for values of α not equal to α^* or the transition to the late-time swelling-dominated mechanisms. To do this, we relax our assumption that $\varphi = 0$ and assume that swelling and drying must play a role in all cases aside from $\alpha = \alpha^*$. Treating the gel layer as uniform with polymer fraction

$$\bar{\Phi} = \int_0^1 \Phi(u,\, t)\, du \quad (\approx \Phi^* \text{ as } \tau \to 0), \tag{66}$$

but with a nonzero gradient Φ_y at $y = 1$, we solve the same problem as in Sec. IV with the inhomogeneous pervadic pressure boundary condition of Eq. (51) to find the dispersion relation,

$$2\bar{\Phi}[D\bar{\Phi}^{-\frac{1}{2}}\Phi_y - 2(\mathcal{M}+\bar{\Phi}-1)s]\alpha^2 - 2\mathcal{M}\bar{\Phi}[s + 2\bar{\Phi}^{\frac{1}{2}}(\mathcal{M}+\bar{\Phi}-1)]\alpha\sinh(2\alpha) - D\Phi_y(s + 2\mathcal{M}\bar{\Phi}^{\frac{1}{2}}\alpha^2)\cosh(2\alpha)$$
$$+ 4\mathcal{M}\bar{\Phi}^{\frac{1}{2}}\alpha\cosh\alpha\tanh\left(\sqrt{\alpha^2 + \frac{s}{D}}\right)[2\bar{\Phi}(\mathcal{M}+\bar{\Phi}-1)\alpha\cosh\alpha + D\Phi_y\sinh\alpha]\sqrt{\alpha^2+\frac{s}{D}} + sD\Phi_y = 0, \tag{67}$$

where $D = D(\bar{\Phi})$ (as described in Appendix B 2). First, we can set s to zero to find the marginally stable curve,

$$\mathcal{M}(1 + \bar{\Phi}^{1/2} - \bar{\Phi})\sinh(2\alpha) + 2\bar{\Phi}^{1/2}(\mathcal{M}+\bar{\Phi}-1)\alpha$$
$$= (1 + \mathcal{M}\bar{\Phi}^{-1/2})\left(\tanh\alpha - \bar{\Phi}^{1/2}\frac{\sinh^2\alpha}{\alpha}\right)\Phi_y. \tag{68}$$

This relation, shown in Fig. 12(a), illustrates yet again how the interfacial polymer fraction gradient destabilizes otherwise stable situations. These marginal curves also explain why instability is seen for a finite band of wave numbers at intermediate times in Fig. 10(b), provided $\Phi_y < 0$, there is a band of wave numbers which are unstable with polymer fractions $\bar{\Phi} < \Phi_{\text{crit}}$. At any given stage in the swelling, denote the minimum value of $\bar{\Phi}$ for which there exists an instability (i.e., the minimum point on the marginal stability curve) $\bar{\Phi}_{\text{crit}}$, and so the criterion for an instability to exist becomes $\bar{\Phi} \geqslant \bar{\Phi}_{\text{crit}}$. Notice that $\bar{\Phi}_{\text{crit}} \leqslant \Phi_{\text{crit}}$, with equality if and only if $\Phi_y = 0$.

Solving Eq. (68) with $\bar{\Phi} = 1$ implies that all gels, irrespective of polymer fraction, are unstable when

$$|\Phi_y| \geqslant \frac{5.194\mathcal{M}}{1+\mathcal{M}} \quad \text{or} \quad \delta \lesssim \frac{1+\mathcal{M}}{5.194\mathcal{M}(\Phi^* - \Phi_1)}. \tag{69}$$

This explains that instability occurs at all polymer fractions, provided that $|\Phi_y|$ is sufficiently large. Figure 12(b) illustrates how the criterion for instability becomes stricter as the magnitude of Φ_y drops.

In addition, we can recover the buckling instability in this intermediate-time regime by taking the dominant balance of the dispersion relation (67) when $s \to \infty$,

$$\frac{D\Phi_y}{\bar{\Phi}}\sinh^2(\alpha) + 2(\mathcal{M}+\bar{\Phi}-1)\alpha^2 + \mathcal{M}\alpha\sinh(2\alpha) = 0. \tag{70}$$

Comparing the predictions of Eq. (70) and (54) for different values of Φ_y in Fig. 13, we see excellent agreement as $\Phi_y \to -\infty$ (i.e., early times in the swelling process, when the first and third terms are the dominant balance) but some divergence as the magnitude of the interfacial polymer fraction gradient decreases and the thickness of the boundary layer increases, necessitating some compressible component to the instability, as found in this intermediate-time solution, but not seen in the early-time relation. Physically, this corresponds to a need to match tangential stresses with the water above as the swollen boundary layer thickens, a boundary condition we neglected in the early-time approximation, but can no longer ignore if the there is no thin, clearly defined, "skin."

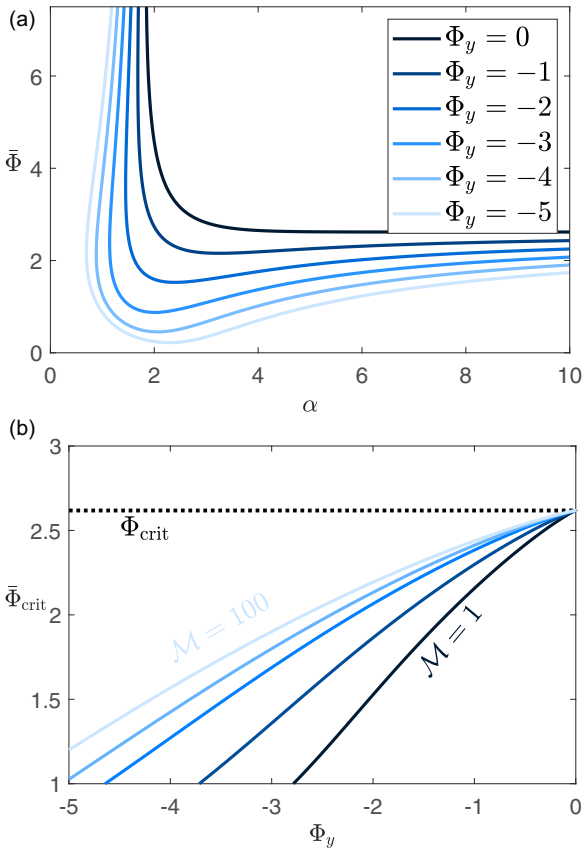

FIG. 12. (a) A plot of the marginally stable modes for different values of Φ_y when $\mathcal{M} = 1$ for different values of Φ_y, showing how the transient swelling state destabilizes some wave numbers α where $\bar{\Phi} < \Phi_{\text{crit}}$. (b) A plot of the critical value of $\bar{\Phi}$ above which instabilities of some wave numbers are seen, corresponding to Φ_{crit} in the fully swollen case. Notice how, at early times when $\Phi_y \to -\infty$, the criterion for an instability is weaker.

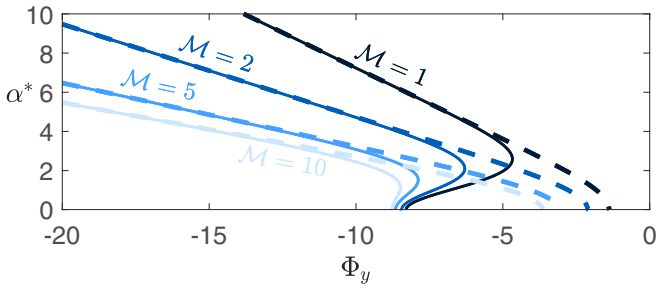

FIG. 13. Comparisons of the early-time approximation for α^* (dashed curves) from Eq. (54) with the intermediate-time solutions (70) that allow for some compressibility (solid curves). In all cases, $\Phi^* = 5$.

Since the early-time approximation found for a purely elastic instability is likely to be invalid as the gel swells further and the boundary layer thickens, the approximation for the critical value of δ at which a buckling instability ceases to be possible is likely better approximated by finding the maximum value of Φ_y for which a solution $\alpha = \alpha^*$ can be found to Eq. (70). Figure 14 shows this value of δ_c, illustrating how decreasing $\mathcal{M}$ and increasing $\bar{\Phi}$ lead to a greater thickness of the swollen layer before the buckling instability ceases to exist.

Unlike in the early-time case, α^* does not equal zero at $\delta = \delta_c$, as seen in the position of the turning points of the solid curves in Fig. 13. The value of α^* when the system transitions from buckling to swelling is denoted α_∞ and can be expected to be the wave number seen for all time once these fast instabilities no longer occur. Tanaka *et al.* [21] saw in their experiments that the most unstable wavelength increased with the square root of time, before reaching a final value that remained roughly constant for all time, and we propose that this is equal to the α_∞ predicted by our model, since any

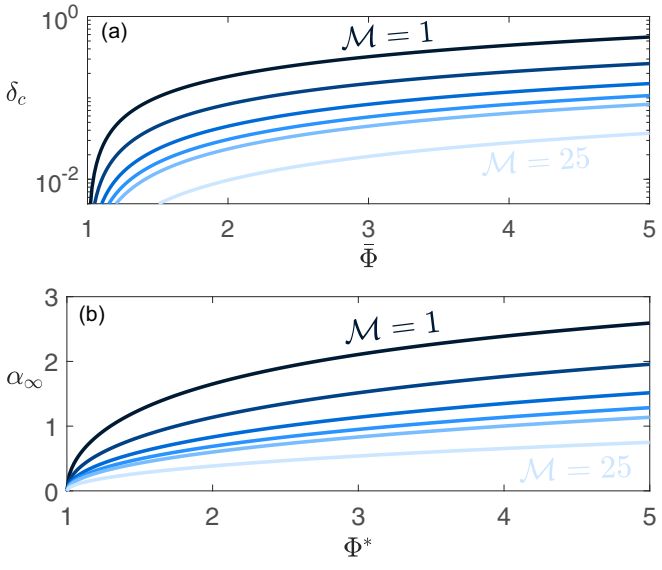

FIG. 14. (a) Plots of δ_c for different values of $\bar{\Phi}$ and $\mathcal{M}$, showing the critical swollen layer thickness beyond which buckling instabilities no longer occur. (b) Plots of α_∞, the final value of α^* when $\delta = \delta_c$, again shown for different $\mathcal{M}$ and Φ^*.

wrinkling instabilities at late times grow by the much slower process of swelling and therefore are likely to have little net effect on the steady-state morphology. These values of α_∞ are plotted in Fig. 14(b), showing how the late-time wave number depends on material properties and Φ^*.

E. Changing behavior of the instability in time

In the preceding sections, we have deduced properties of the buckling and swelling instabilities in terms of the thickness $\delta = \Delta/a(\tau)$ of the swollen layer of the gel, where we know that $\delta \to 1$ as $\tau \to \infty$ and $\delta \to 0$ as $\tau \to 0$. The similarity solution for the base state derived in Sec. II C allows us to deduce the dependence of δ on time as the gel approaches its late-time steady state, and therefore we can take

$$\delta = \frac{a(\tau) - a^*}{a(\tau)} \approx 2\lambda\sqrt{D(\Phi^*)\tau} \quad \text{as } \tau \to 0. \tag{71}$$

At the very earliest of times, there is always a buckling instability, irrespective of the composition of the gel or its material properties, as shown in Eq. (69). The wavelength of this instability scales like the thickness of the swollen layer at the earliest times, as shown in Eq. (57), and so

$$\alpha^* \approx \frac{1}{4\lambda\mathcal{M}}\left(1 - \frac{\Phi_1}{\Phi^*}\right)\sqrt{\frac{D(\Phi^*)}{\tau}}. \tag{72}$$

Viewing this early-time wrinkling in terms of time and not δ makes it clear how the wave-number evolution seen by Tanaka *et al.* [21] arises and explains the $\alpha^* \propto \tau^{-1/2}$ behavior seen in Fig. 11.

We can now describe the transition in between the different forms of instability in terms of two critical times. In all cases, the interface is linearly unstable immediately after being brought into contact with water, until δ reaches δ_c at a time $\tau = \tau_{\text{buckle}}$. Beyond this time, there is no longer an elastically driven instability, and any instability (if it exists) is purely swelling driven. The surface remains linearly unstable if $\Phi_1 > \Phi_{\text{crit}}$, but in other cases the interface is not unstable when $|\Phi_y|$ becomes too small to support an instability, and we transition to a state where the interface is stable to small perturbations at a time τ_{stable}. This explains the observations that the interface can "heal" in time—though the process of smoothing out the wrinkles is not modelled here, since it would rely on nonlinear effects, the surface is no longer unstable to small perturbations and so wrinkles will no longer grow. There is therefore a possibility that the interface can return to a smooth planar state as the gel continues to swell in these cases, and this is seen in experiments as a smoothing or healing when the system transitions to a linearly stable nature. Figure 15 shows this time-varying behavior in a phase diagram, with all gels starting out unstable, with later transitions to swelling-moderated wrinkling and/or healing.

VI. CONCLUSIONS

The quantity of experimental and theoretical investigations into the wrinkling instability of surface-attached gels is testament to the rich variety of behavior exhibited by this seemingly simple phenomenon, providing insights into the constitutive modeling of hydrogels, the diffusive mechanisms driving flow into and out of the polymer matrix and the elastic

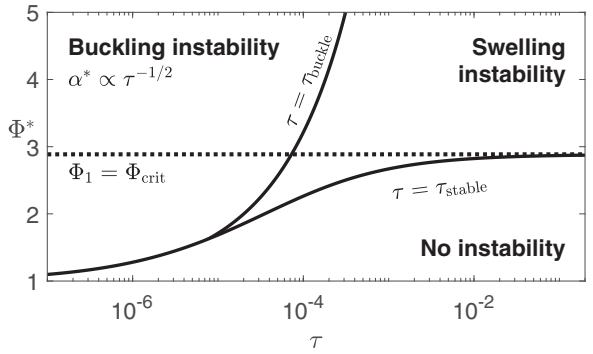

FIG. 15. Plots of the different stability properties for a gel where $\mathcal{M} = 10$ and how these depend on time τ and initial polymer fraction Φ^*. To produce this plot, a full numerical solution has been used to deduce $\bar{\Phi}$, so that the solution remains valid for larger values of τ.

anchoring effects provided by the constraints. In this paper, we have shown how the key behaviors observed in experiments beginning with those of Tanaka *et al.* [19] can be explained by taking a linear-elastic-nonlinear-swelling model for the gel and describing the growth of wrinkles as a diffusive process, with water being driven into the gel due to gradients in pervadic (pore) pressure.

In contrast to other existing models of the wrinkling process (for example, Kang and Huang [22] or Tanaka *et al.* [19]), this emphasis on the swelling mechanism behind the growth of instabilities (at all but the earliest times) allows us to deduce a growth rate for an instability of any given wave number, through a dispersion relation describing growth rate as a function of wave number and material properties. In this sense, our analysis is akin to the vast array of stability analyses found in the fluid mechanics literature (e.g., Drazin and Reid [29]) and allows us to find more than a criterion for exchange of stability as calculated by Kang and Huang [22]. Specifically, we show that the fixed base stabilizes long-wavelength wrinkles such that there is a minimum wave number at which an instability is seen, but that there is no stabilizing mechanism for shorter-wavelength wrinkles and the fastest-growing modes have infinite wave number. This is clearly unphysical and requires regularization. Other authors have suggested processes such as surface tension to provide this stabilization [24], but we have not investigated its effect here.

Perhaps the most remarkable behavior seen in experiments is the smoothing and healing of wrinkles as swelling continues. With an understanding of the evolution of the base state, it is possible to investigate the key characteristics of the wrinkling instability on different timescales; the early-time elastically dominated instability, the swelling-moderated wrinkling at intermediate times, destabilized by interfacial gradients in Φ, and then the potential healing of instabilities as the steady state $\Phi \equiv \Phi_1$ is approached. Figure 15 illustrates the three different ways in which a surface instability can evolve. First, the initial polymer fraction may be sufficiently low that compressive stresses are comparatively small, and a buckling instability occurs which then heals, and the final state is stable (in effect, $\tau_{\text{buckle}} = \tau_{\text{stable}}$). Intermediate polymer fractions, where $\Phi_1 < \Phi_{\text{crit}}$ still, start out as buckling instabilities, progress to swelling instabilities, and then heal. Finally, if $\Phi_1 > \Phi_{\text{crit}}$, then the instability starts out as incompressible elastic buckling and then there is a persistent swelling instability.

It has been postulated by other authors that the characteristic lengthscale of the wrinkles in the experiment increases with the thickness of the diffusively swollen layer, which would suggest a wrinkle wavelength that initially increases with the square root of time, and we have shown that this is indeed the case. At very early times, it is seen that the mechanism underlying the instability is distinct from that at later times, with the pervadic pressure boundary condition imposing a normal stress condition on the surface, but the resultant instability is purely elastic in its growth. Some authors, such as Tanaka *et al.* [20], notice a later phase of wavelength growth, where the characteristic wavelength increases like the cube root of time, and we speculate that this arises from a coarsening or ripening effect that is nonlinear in nature and thus not captured in our context.

Though this model provides a description of all the key features seen in experiments, in order to better understand the evolution of the wrinkled patterns, including the formation of sharp creases and folds as seen by Trujillo *et al.* [18], it is likely that a nonlinear stability analysis is necessary to understand the evolution of these more complicated patterns. Our current understanding of the late-time instability also lacks a stabilizing process for short-wavelength wrinkles, with an ultraviolet catastrophe giving maximum growth rates as $\alpha \to \infty$. However, it is likely that the wavelength selection made at early times (when the instability is elastically dominated and the growth rates are faster) sets the lengthscale at later times, with $\alpha \approx \alpha_\infty$ for all times once buckling instabilities are no longer possible, and this is indeed attested to by experimental evidence [21].

ACKNOWLEDGMENTS

J.J.W. was supported by the Natural Environment Research Council (project reference 2436164) through the Cambridge Climate, Life and Earth Sciences DTP (NE/S007164/1) for this research.

APPENDIX A: FINDING EXPLICIT EIGENFUNCTIONS

In the uniformly swollen case, it is possible to find analytic eigenfunctions for the displacement, polymer fraction, and pervadic pressure fields, illustrating the form of the solution more clearly than a purely numerical approach. Assuming from hereon in that $\Phi \equiv \Phi_1$, a constant, with $D = D(\Phi_1)$, the governing equations (45) reduce to

$$\mathcal{M}\left(\frac{\partial^2}{\partial y^2} - \alpha^2\right)\eta = \frac{\partial p}{\partial y} + \frac{\partial \varphi}{\partial y}, \tag{A1a}$$

$$\left(\frac{\partial^2}{\partial y^2} - \alpha^2\right)(D\varphi + \Phi_1 p) = 0, \tag{A1b}$$

$$\left(\frac{\partial^2}{\partial y^2} - \alpha^2 - \frac{s}{D}\right)\varphi = 0, \tag{A1c}$$

$$\left.\begin{aligned} \eta = \tfrac{\partial \varphi}{\partial y} = 0, \\ \tfrac{\partial p}{\partial y} = 0. \end{aligned}\right\} \quad \text{on } y = 0. \tag{A1d}$$

$$\left.\begin{aligned} p &= 0, \\ (D/\Phi_1)\tfrac{\partial \varphi}{\partial y} + \tfrac{\partial p}{\partial y} + 2(\mathcal{M}+\Phi_1-1)\alpha^2\eta, \\ 2\mathcal{M}\tfrac{\partial \eta}{\partial y} &= \left(1-\mathcal{M}\Phi_1^{-1/2}\right)\varphi. \end{aligned}\right\} \quad \text{on} \quad y=1. \tag{A1e}$$

Then, on the assumption that $s \neq 0$,

$$\varphi = C_1 \cosh\left(\sqrt{\alpha^2 + \frac{s}{D}}\, y\right) \quad \text{and} \tag{A2a}$$

$$p = C_2 \cosh(\alpha y) - \frac{DC_1}{\Phi_1}\cosh\left(\sqrt{\alpha^2+\frac{s}{D}}\, y\right), \tag{A2b}$$

with a vertical displacement given by

$$\eta = \left(C_3 - \frac{C_2}{4\mathcal{M}\alpha}\right)\sinh(\alpha y) + \frac{C_2 y}{2\mathcal{M}}\cosh(\alpha y) - \frac{C_1 D \Phi^{-1/2}}{s}\sqrt{\cdot}\,\sinh\left(\sqrt{\cdot}\, y\right), \tag{A2c}$$

where $\sqrt{\cdot}$ is shorthand for $\sqrt{\alpha^2 + s/D}$. Since we are seeking eigenfunction solutions, we can impose an arbitrary normalization on φ, η and p, so we choose $\eta = 1$ on $y = 1$. The first two boundary conditions on $y = 1$ imply that

$$\varphi = -\frac{2\Phi_1\alpha(\mathcal{M}+\Phi_1-1)}{D\tanh\alpha}\frac{\cosh(\sqrt{\cdot}\, y)}{\cosh(\sqrt{\cdot})} \quad \text{and} \tag{A3a}$$

$$p = \frac{2\alpha(\mathcal{M}+\Phi_1-1)}{\tanh\alpha}\left[\frac{\cosh(\sqrt{\cdot}\, y)}{\cosh(\sqrt{\cdot})} - \frac{\cosh(\alpha y)}{\cosh\alpha}\right], \tag{A3b}$$

alongside the vertical displacement eigenfunction, having imposed $\eta(1) = 1$,

$$\eta = \left\{1 + \frac{(\mathcal{M}+\Phi_1-1)\left[s - 2\mathcal{M}\Phi_1^{1/2}\sqrt{\cdot}\tanh(\sqrt{\cdot})\right]\alpha}{\mathcal{M}s\tanh\alpha}\right\} \times \frac{\sinh(\alpha y)}{\sinh\alpha} + \frac{2\Phi_1^{1/2}(\mathcal{M}+\Phi_1-1)}{s}\frac{\alpha\sqrt{\cdot}}{\tanh\alpha}\frac{\sinh(\sqrt{\cdot}\, y)}{\cosh\sqrt{\cdot}} - \frac{\mathcal{M}+\Phi_1-1}{\mathcal{M}}\frac{\alpha y\cosh(\alpha y)}{\sinh\alpha}. \tag{A3c}$$

These solutions can then be substituted into the third interfacial boundary condition to retrieve the dispersion relation of Eq. (49).

All three perturbation eigenfunctions are plotted in Fig. 7, showing decay away from the top boundary on the nondimensional lengthscale α^{-1}, as would be expected given that all are dependent on $\exp(\pm\alpha y)$. If $s = 0$, then we can repeat this process to find the eigenfunctions in the marginally stable case.

APPENDIX B: MATRIX FORMULATION OF THE PERTURBATION EQUATIONS

The governing equations (45) are linear in the perturbation quantities and can therefore be reformulated as a sixth-order matrix system for ease of numerical solution, with $\mathbf{X} = (\eta,\ \varphi,\ p,\ \eta',\ \varphi',\ p')^T$, where primes here denote derivatives with respect to y. The solution vector $\mathbf{X}$ satisfies $\partial\mathbf{X}/\partial y = \mathbf{M}\mathbf{X}$ with

$$\begin{aligned} &\mathsf{M}_{14} = 1 \quad \mathsf{M}_{25} = 1 \quad \mathsf{M}_{36} = 1 \\ &\mathsf{M}_{41} = \alpha^2 \quad \mathsf{M}_{45} = 1/\mathcal{M} \quad \mathsf{M}_{46} = 1/\mathcal{M} \\ &\mathsf{M}_{51} = \frac{s\Phi'}{\Phi^{1/2}D(\Phi)} \quad \mathsf{M}_{52} = \frac{s + D(\Phi)\alpha^2 - \Phi''}{D(\Phi)} + \frac{(3\mathcal{M}+2\Phi^{1/2})\Phi'^2 - 2\mathcal{M}\Phi\Phi''}{4\Phi^{3/2}D(\Phi)} \\ &\mathsf{M}_{55} = -\frac{(2+\mathcal{M}\Phi^{-1/2})\Phi'}{D(\Phi)} \quad \mathsf{M}_{56} = -\frac{\Phi'}{D(\Phi)} \\ &\mathsf{M}_{61} = -\frac{s\Phi'}{\Phi^{3/2}} \quad \mathsf{M}_{62} = \frac{D(\Phi)\Phi'' - \Phi'^2/2 - s\Phi}{\Phi^2} - \frac{3\mathcal{M}\Phi'^2}{2\Phi^{5/2}} \\ &\mathsf{M}_{63} = \alpha^2 \quad \mathsf{M}_{65} = \frac{2D(\Phi)\Phi'}{\Phi^2} \quad \mathsf{M}_{66} = \frac{\Phi'}{\Phi}, \end{aligned} \tag{B1}$$

all other matrix elements being zero, with $\Phi' = \partial\Phi/\partial y$. Furthermore, the basal and interfacial boundary conditions can be imposed by taking $\mathbf{B_0}\mathbf{X_0} = \mathbf{B_1}\mathbf{X_1} = \mathbf{0}$, where $\mathbf{X_0}$ and $\mathbf{X_1}$ are the values of $\mathbf{X}$ at $y = 0$ and $y = 1$, respectively, and

$$\mathbf{B_0} = \begin{pmatrix} 0 & 1 & 0 & 0 & 0 & 0 \\ 0 & 0 & 0 & 0 & 1 & 0 \\ 0 & 0 & 0 & 0 & 0 & 1 \end{pmatrix} \quad \text{and}$$

$$\mathbf{B_1} = \begin{pmatrix} -\frac{D(\Phi_1)}{\Phi_1}\Phi' & 0 & 1 & 0 & 0 & 0 \\ \mathsf{B}_{121} & -\frac{\mathcal{M}\Phi'}{2\Phi_1^{3/2}} & 0 & 0 & \frac{D(\Phi_1)}{\Phi_1} & 1 \\ \frac{D(\Phi_1)\Phi'}{\Phi_1} & \mathsf{B}_{132} & 0 & 2\mathcal{M} & 0 & 0 \end{pmatrix}, \tag{B2}$$

where $\mathsf{B}_{121} = 2(\mathcal{M}+\Phi_1-1)\alpha^2$ and $\mathsf{B}_{132} = \mathcal{M}\Phi_1^{-1/2} - 1$. This system of equations is solved in MATLAB using the `bvp4c` solver [30].

1. Uniform polymer fraction

When $\Phi \equiv \Phi_1$, the matrix $\mathbf{M}$ is a constant, and therefore the general solution to the governing equations can be expressed as a matrix exponential

$$\mathbf{X} = \exp[\mathbf{M}y]\mathbf{X_0}, \tag{B3}$$

and, imposing $\eta = \partial\varphi/\partial y = \partial p/\partial y = 0$ on $y = 0$, $\mathbf{X_0}$ must take the form $(0,\ 0,\ c_1,\ c_2,\ c_3,\ 0)^T$, for c_i constants. Then,

$$\mathbf{X_1} = \exp[\mathbf{M}](0,\ 0,\ c_1,\ c_2,\ c_3,\ 0)^T, \tag{B4}$$

and the condition for a nontrivial perturbation solution to exist with wave number α and growth rate s is simply that there exists a solution $(c_1,\ c_2,\ c_3)^T$ to $\mathbf{B_1}\mathbf{X_1} = \mathbf{0}$ that is nonzero. A criterion for this can be determined by rewriting $\mathbf{B_1}\mathbf{X_1} = \mathbf{0}$ in the form $\mathbf{C}(c_1,\ c_2,\ c_3)^T = \mathbf{0}$, where

$$\mathbf{C} = \mathbf{B_1}\exp[\mathbf{M}]\begin{pmatrix} 0 & 0 & 1 & 0 & 0 & 0 \\ 0 & 0 & 0 & 1 & 0 & 0 \\ 0 & 0 & 0 & 0 & 1 & 0 \end{pmatrix}^T, \tag{B5}$$

and solving

$$\det \mathbf{C} = 0, \tag{B6}$$

giving the dispersion relation of Eq. (49).

2. Early-time approximation

In this approximation, we solve the same governing equations as with the uniform polymer fraction but impose a different pervadic pressure boundary condition. Thus, $\mathbf{M}$ is the same as in Sec. B 1 with all instances of Φ_1 replaced by $\bar{\Phi}$. Therefore,

$$\mathbf{X_1} = \exp[\mathbf{M}](0,\ 0,\ c_1,\ c_2,\ c_3,\ 0)^T, \tag{B7}$$

with the boundary conditions to be imposed at $y = 1$ described by

$$\mathbf{B_1} = \begin{pmatrix} -\frac{D(\bar{\Phi})}{\bar{\Phi}}\Phi_y & 0 & 1 & 0 & 0 & 0 \\ \mathsf{B}_{121} & 0 & 0 & 0 & \frac{D(\bar{\Phi})}{\bar{\Phi}} & 1 \\ 0 & \mathsf{B}_{132} & 0 & 2\mathcal{M} & 0 & 0 \end{pmatrix}, \tag{B8}$$

with Φ_y the value of $\partial\Phi/\partial y$ at $y = 1$ and B_{121} and B_{132} as in Eq. (B2) but with Φ_1 replaced by $\bar{\Phi}$. The dispersion relation in Eq. (67) is obtained by rewriting the condition $\mathbf{B_1 X_1} = \mathbf{0}$ as a matrix equation for $(c_1,\ c_2,\ c_3)^T$ and seeking the criterion for a nonzero solution to exist.

[1] E. Cerda and L. Mahadevan, Geometry and physics of wrinkling, Phys. Rev. Lett. **90**, 074302 (2003).

[2] M. Ben Amar and A. Bordner, Mimicking cortex convolutions through the wrinkling of growing soft bilayers, J. Elast. **129**, 213 (2017).

[3] L. Ronan, N. Voets, C. Rua, A. Alexander-Bloch, M. Hough, C. Mackay, T. J. Crow, A. James, J. N. Giedd, and P. C. Fletcher, Differential tangential expansion as a mechanism for cortical gyrification, Cereb. Cortex **24**, 2219 (2014).

[4] H. H. Dai and Y. Liu, Critical thickness ratio for buckled and wrinkled fruits and vegetables, Europhys. Lett. **108**, 44003 (2014).

[5] M. Gomez, D. E. Moulton, and D. Vella, Critical slowing down in purely elastic snap-through instabilities, Nat. Phys. **13**, 142 (2017).

[6] S. P. Timoshenko and J. M. Gere, *Theory of Elastic Stability* (McGraw-Hill, New York, 1961).

[7] M. A. Biot, Surface instability of rubber in compression, Appl. Sci. Res. **12**, 168 (1963).

[8] H. Alawiye, E. Kuhl, and A. Goriely, Revisiting the wrinkling of elastic bilayers I: linear analysis, Philos. Trans. R. Soc. London A **377**, 20180076 (2019).

[9] J. Groenewold, Wrinkling of plates coupled with soft elastic media, Physica A **298**, 32 (2001).

[10] J. Dervaux, Y. Couder, M. A. Guedeau-Boudeville, and M. Ben Amar, Shape transition in artificial tumors: From smooth buckles to singular creases, Phys. Rev. Lett. **107**, 018103 (2011).

[11] M. Ben Amar, Creases and cusps in growing soft matter, arXiv:2309.11412.

[12] M. A. Etzold, G. T. Fortune, J. R. Landel, and S. B. Dalziel, Droplet absorption and spreading into thin layers of polymer hydrogels, J. Fluid Mech. **974**, A7 (2023).

[13] A. I. Poland and J. T. Gosling, Reticulation: Effects and cure, AAS Photo Bull. **2**, 14 (1975).

[14] T. Bertrand, J. Peixinho, S. Mukhopadhyay, and C. W. MacMinn, Dynamics of swelling and drying in a spherical gel, Phys. Rev. Appl. **6**, 064010 (2016).

[15] C. M. González-Henríquez, M. A. Sarabia Vallejos, and J. Rodríguez-Hernández, Wrinkled surfaces designed for biorelated spplications, in *Wrinkled Polymer Surfaces: Strategies, Methods and Applications*, edited by C. M. González-Henríquez and J. Rodríguez-Hernández (Springer International, Cham, 2019), pp. 273–290.

[16] E. P. Chan, E. J. Smith, R. C. Hayward, and A. J. Crosby, Surface wrinkles for smart adhesion, Adv. Mater. **20**, 711 (2008).

[17] C. Y. Liaw, J. Pereyra, and M. Guvendiren, Wrinkling on covalently anchored hydrogels, in *Wrinkled Polymer Surfaces: Strategies, Methods and Applications*, edited by C. M. González-Henríquez and J. Rodríguez-Hernández (Springer International, Cham, 2019), pp. 205–227.

[18] V. Trujillo, J. Kim, and R. C. Hayward, Creasing instability of surface-attached hydrogels, Soft Matter **4**, 564 (2008).

[19] T. Tanaka, S. T. Sun, Y. Hirokawa, S. Katayama, J. Kucera, Y. Hirose, and T. Amiya, Mechanical instability of gels at the phase transition, Nature (London) **325**, 796 (1987).

[20] T. Tanaka, S. T. Sun, Y. Hirokawa, S. Katayama, J. Kucera, Y. Hirose, and T. Amiya, Mechanical instability of swelling gels, in *Studies in Polymer Science*, edited by M. Nagasawa, Volume 2 of Molecular Conformation and Dynamics of Macromolecules in Condensed Systems (Elsevier, Amsterdam, 1988), pp. 203–222.

[21] H. Tanaka, H. Tomita, A. Takasu, T. Hayashi, and T. Nishi, Morphological and kinetic evolution of surface patterns in gels during the swelling process: Evidence of dynamic pattern ordering, Phys. Rev. Lett. **68**, 2794 (1992).

[22] M. K. Kang and R. Huang, Swell-induced surface instability of confined hydrogel layers on substrates, J. Mech. Phys. Solids **58**, 1582 (2010b).

[23] W. Hong, X. Zhao, J. Zhou, and Z. Suo, A theory of coupled diffusion and large deformation in polymeric gels, J. Mech. Phys. Solids **56**, 1779 (2008).

[24] M. K. Kang and R. Huang, Effect of surface tension on swell-induced surface instability of substrate-confined hydrogel layers, Soft Matter **6**, 5736 (2010).

[25] J. J. Webber and M. G. Worster, A linear-elastic-nonlinear-swelling theory for hydrogels. Part 1. Modelling of superabsorbent gels, J. Fluid Mech. **960**, A37 (2023).

[26] J. J. Webber, M. A. Etzold, and M. G. Worster, A linear-elastic-nonlinear-swelling theory for hydrogels. Part 2. Displacement formulation, J. Fluid Mech. **960**, A38 (2023).

[27] S. S. L. Peppin, J. A. W. Elliott, and M. G. Worster, Pressure and relative motion in colloidal suspensions, Phys. Fluids **17**, 053301 (2005).

[28] H. F. Wang, *Theory of Linear Poroelasticity with Applications to Geomechanics and Hydrogeology* (Princeton University Press, Princeton, NJ, 2000).

[29] P. G. Drazin and W. H. Reid, Hydrodynamic Stability, *Cambridge Mathematical Library*, 2nd ed. (Cambridge University Press, Cambridge, UK, 2004).

[30] J. Kierzenka and L. F. Shampine, A BVP solver based on residual control and the Matlab PSE, ACM Trans. Math. Softw. **27**, 299 (2001).